Climate change impacts on a eutrophying lake: Cultus Lake, British Columbia, Canada

by

Mark Gregory Sumka

B.Sc., University of Alberta, 2014

A THESIS SUBMITTED IN PARTIAL FULFILLMENT OF
THE REQUIREMENTS FOR THE DEGREE OF

MASTER OF APPLIED SCIENCE

in

The Faculty of Graduate and Postdoctoral Studies

(Civil Engineering)

THE UNIVERSITY OF BRITISH COLUMBIA

(Vancouver)

August 2017

Abstract

This study characterizes the thermal dynamics of Cultus Lake, British Columbia, Canada, and assesses the impacts of climate change on critical habitat for species-at-risk Sockeye Salmon (*Onchorynchus nerka*) and Cultus Lake Pygmy Sculpin (*Cottus aleuticus*). Historical field data spanning 1920s–1930s, 2001–2003, and 2009–2016 were analyzed and a one-dimensional hydrodynamic model (General Lake Model) was calibrated using field data collected in 2016, and validated using field data from 2001–2003 and 2009–2016. The thermal structure of the lake was simulated to 2100 using outputs from the downscaled Canadian Regional Climate Model (CanRCM4) for two climate change scenarios (RCP4.5, moderate emissions scenario; and RCP8.5, extreme emissions scenario). Historically (1923–2016), the total lake heat content increased at a rate of 0.80 $MJ\,m^{-2}\,a^{-1}$ and is projected to warm by 2.0 $MJ\,m^{-2}\,a^{-1}$ (4.2 $MJ\,m^{-2}\,a^{-1}$) for RCP4.5 (RCP8.5). Historically, the Schmidt stability increased by 2.2 $J\,m^{-2}\,a^{-1}$ and is projected to increase by 2.6 $J\,m^{-2}\,a^{-1}$ (6.5 $J\,m^{-2}\,a^{-1}$) for RCP 4.5 (RCP8.5). The duration of stratification has historically been increasing at a rate of 0.18 $d\,a^{-1}$ and is projected to increase by 0.18 $d\,a^{-1}$ (0.50 $d\,a^{-1}$) for RCP4.5 (RCP8.5). The onset of stratification is now two weeks earlier than the 1920s–1930s and currently occurs around 23 March while the breakup date has not changed and occurs around 15 December. However, it is predicted that there will be no change in the date of onset of stratification while breakup will be delayed to 12 January (25 January) for RCP4.5 (RCP8.5). Lake surface temperature and outflow temperature is most important for salmon survival in August through November corresponding with the salmon run. Historical change in mean monthly temperature ranged from 0 $°C\,a^{-1}$ in November to a maximum of 0.016 $°C\,a^{-1}$ in August. This is predicted to increase to 0.016 $°C\,a^{-1}$ (0.046 $°C\,a^{-1}$) in November and 0.031 $°C\,a^{-1}$ (0.069 $°C\,a^{-1}$) in August for RCP4.5 (RCP8.5). Projections indicate fundamental changes to the thermal characteristics of Cultus Lake, which may further degrade water quality, particularly in conjunction with ongoing eutrophication, eliciting fundamental changes in the structural and functional attributes of critical habitat for species-at-risk.

Lay Summary

Cultus Lake is a popular recreational lake located in the eastern Fraser Valley, British Columbia, Canada. Previous studies indicate increased nutrient loading to the lake, resulting in ongoing cultural eutrophication. Changes in the ecosystem are changing habitat for two species at risk of extinction: Sockeye Salmon and Cultus Lake Pygmy Sculpin. The objectives of this study are to 1) characterize the thermal characteristics of this warm monomictic lake; 2) track changes since the early 20^{th} century; and 3) forecast how Cultus Lake may respond to future climate change. Field data collected in 2016 were used to calibrate a numerical model, which was validated on historical measurements and used to forecast the thermal characteristics of the lake under different warming scenarios. Increased warming of the lake is expected to result in habitat modification and loss for two Canadian fish species at risk of extinction.

Preface

This dissertation is an original, unpublished work by the author, Mark Sumka. The field campaign was designed and organised by myself. I also conducted all field data analysis, and data analysis including the model calibration, validation, evaluation, and forecasting scenarios. Assistance for the field campaign was provided principally by members of the UBC Environmental Fluid Mechanics Group: Samuel Brenner, Kelly Graves, David Hurley, and Christopher Young, as well as Dr. Daniel Selbie of Fisheries and Oceans Canada. Dr. Selbie, Kelly Malange, Garrett Lidin, and Kristy Grant from Fisheries and Oceans Canada provided historical lake and river data, a vessel, and equipment for this research. Bathymetric data were provided by the Canadian Hydrographic Service. Historical lake water levels were provided by the Cultus Lake Park Board. Alain Royer, Norm O'Neill, Ihab Abboud, and Vitali Fioletov establish and maintain the air quality monitoring station at Saturna Island.

Table of Contents

Abstract ii

Lay Summary iii

Preface iv

Table of Contents v

List of Tables vii

List of Figures viii

Acknowledgements ix

1 Introduction 1
- 1.1 Seasonal Thermal Stratification of Lakes 2
- 1.2 Climate Change and Lakes 3
- 1.3 Cultus Lake 5
- 1.4 Thesis Objectives 6

2 Methods 8
- 2.1 Site Description 8
- 2.2 Data Collection 11
  - 2.2.1 Historical Data 11
  - 2.2.2 Meteorological Data 11
  - 2.2.3 Limnological Data 14
  - 2.2.4 Water Clarity and Extinction Coefficient 18
  - 2.2.5 Inflows and Outflow 18
- 2.3 General Lake Model (GLM) 20
  - 2.3.1 Model Description 20
  - 2.3.2 Model Setup 22
- 2.4 Regional Climate Model 24
  - 2.4.1 Forecast Data 24

3 Results . . . 27
3.1 Temperature . . . 27
3.2 Conductivity . . . 32
3.3 Water Clarity and Chlorophyll-a . . . 33
3.4 Inflows and Outflow . . . 34
3.5 Modelling Cultus Lake . . . 38
3.5.1 Calibration Period . . . 38
3.5.2 Model Evaluation . . . 40
3.5.3 Sensitivity Analysis . . . 45
3.5.4 Hindcast (2009–2016) . . . 46
3.5.5 Forecast Data Evaluation (2001–2003) . . . 49
3.6 Historical and Forecast Results (1923–2100) . . . 53
3.6.1 Heat Content . . . 53
3.6.2 Stability and Stratification . . . 55
3.6.3 Surface and Outflow Temperatures . . . 61

4 Discussion . . . 63
4.1 Potential Changes to the Lake Mixing Regime . . . 63
4.2 Implications of Increased Climate Warming on Ecosystem Structure and Functioning . . . 65
4.3 Trophic Status of Cultus Lake . . . 67
4.4 Managing the Impacts of Climate Change . . . 70

5 Conclusions . . . 71

Appendix A Inflow and Outflow Descriptions . . . 84

List of Tables

Table 2.1 Accuracy, resolution, and drift of HOBO weather station instruments 13
Table 2.2 Bird clear-sky model atmospheric parameters 14
Table 2.3 Cultus Lake station information 15
Table 2.4 Accuracy, resolution, and drift for SBE 19plus V2 CTD 16
Table 2.5 Stream gauging station information 19
Table 2.6 Stream temperature coefficients 20

Table 3.1 Calibration parameters for GLM setup 39
Table 3.2 Inflow parameters for GLM 40
Table 3.3 Sensitivity analysis results and error between observed and synthetic meteorological data 46
Table 3.4 Comparison of three methods used to calculate the duration of stratification 58

List of Figures

Figure 2.1 Map of Cultus Lake 10
Figure 2.2 Hypsographic curve 17
Figure 2.3 Lake water levels 17

Figure 3.1 Limnological field data results 30
Figure 3.2 Thermistor moorings 31
Figure 3.3 Wind speed, gust, and direction 32
Figure 3.4 Discharge and temperature of Frosst Creek and Sweltzer River, and total daily precipitation at Abbotsford Airport . . 35
Figure 3.5 Discharge for Watt Creek and Smith Falls Creek, and specific conductivity and turbidity for Frosst Creek, Watt Creek, and Smith Falls Creek 37
Figure 3.6 Overlaid observed and simulated temperature profiles 41
Figure 3.7 RMSE for 2016 GLM calibration 43
Figure 3.8 Observed and simulated heat content for 2016 calibration 44
Figure 3.9 RMSE for 2009–2016 hindcast 48
Figure 3.10 Observed and simulated heat content for 2009–2016 hindcast 48
Figure 3.11 RMSE for 2001–2003 hindcast 52
Figure 3.12 Observed and simulated heat content for 2001–2003 hindcast 52
Figure 3.13 Historical and projected heat content 54
Figure 3.14 Historical and projected Schmidt Stability Index . . . 56
Figure 3.15 Thermal stratification calculation method comparison 57
Figure 3.16 Historical and predicted duration of thermal stratification 60
Figure 3.17 Historical and predicted onset and breakup of thermal stratification 60
Figure 3.18 Historical and predicted outflow temperatures 62

Acknowledgements

I would like to thank my supervisor, Dr. Bernard Laval, and Dr. Daniel Selbie for their support and guidance throughout my research. Thank you to the UBC Environment Fluid Mechanics group (Samuel Brenner, Kelly Graves, David Hurley, and Christopher Young) for your assistance with field work. Also, thank you to the Cultus Lake Salmon Research Laboratory staff, in particular Dr. Selbie, Kelly Malange, Garrett Lidin, and Kristy Grant, for providing limnological data, and research equipment, as well as Troy Davis from the Cultus Lake Park Board for providing me with lake level data. I am also grateful to Steve Marks from the Cultus Lake Marina for granting me permission to install a weather station on his roof.

Chapter 1

Introduction

Cultural eutrophication, the artificial fertilization of water bodies with excess nutrients, is the most pervasive problem affecting the water quality of lakes and rivers worldwide (Chambers et al. 2001; D. W. Schindler 2012). Classic symptoms of lake eutrophication include increased aquatic plant and algal growth, and deterioration of fisheries and recreational suitability (Bartsch 1970; Anderson et al. 2002). While eutrophication occurs naturally over very long time scales, many lakes are experiencing rapidly increased eutrophication rates due to nutrient loading from anthropogenic sources such as agriculture, urban runoff, and industrial sources (Bartsch 1970; Anderson et al. 2002; V. H. Smith and D. W. Schindler 2009). Increases in algal-limiting nutrient loading, especially phosphorus and nitrogen, combined with sufficient sunlight penetration in lakes, results in excessive plant and algae growth (cultural eutrophication; Vallentyne (1974) and Anderson et al. (2002)). When plants and algae in lakes senesce, they settle to the bottom where bacterial aerobic decomposition of organic matter occurs (Kankaala et al. 2002), consuming oxygen which can have impacts on deepwater resident fish and benthos (Ficke et al. 2007).

Climate change is amplifying the symptoms of lake eutrophication (Jeppesen et al. 2010; B. Moss et al. 2011). For instance, warmer water temperatures lead to reduced water column mixing, which isolates lake epilimnia from hypolimna over a more protracted period, enhancing hypolimnetic oxygen depletion (Matzinger et al. 2007). Hypoxic deepwater conditions can be accentuated by decomposition of greater amounts of autochthonous organic matter arising from nutrient-stimulated growth of macrophytes (Kankaala et al. 2002) and algae, such as cyanobacteria (O'Neil et al. 2012). Such fundamental abiotic and biotic changes in lakes can elicit upward cascading effects on the lake ecosystem to valued ecosystem components such as fish (Vincent 2009).

This thesis begins with a review of the mechanisms of seasonal thermal stratification of lakes, followed by a review of the effects of climate change on stratification and the potential effects of climate change on cultural eutrophication, narrowing in on the trophic status of Cultus Lake. Chapter 2

provides a description of the site and the fieldwork involved in the development of a one-dimensional Lagrangian hydrodynamic model, the General Lake Model (GLM; Hipsey, Bruce, et al. 2014), along with a description of the forecast model used, Canadian Regional Climate Model (CanRCM4, Environment and Climate Change Canada 2017). Results of the 2016 field campaign are provided in Chapter 3, in addition to modelled results for the 2016 season and model validation using historical data (2001–2003 and 2009–2016). Chapter 3 concludes with a comparison of historical (1923–2016) thermal observations to model hindcasts, and future projections under two climate change scenarios. Chapter 4 describes the possible future mixing conditions in the Cultus Lake under climate change, and associated potential changes to lake ecosystem structure and functioning, with effects on resident and anadromous species, as well as the potential effects of climate change on the trophic status of Cultus Lake. Options to mitigate the ecosystem impacts of climate change through nutrient abatement are explored.

1.1 Seasonal Thermal Stratification of Lakes

Thermal stratification is a physically forced phenomenon that develops seasonally in most deep temperate lakes (Wetzel 2001). Lakes are classified based on their seasonal stratification and mixing regimes where dimictic lakes mix twice annually (in the spring and fall) and monomictic lakes undergo a single annual mixing event (Wetzel 2001). Monomictic lakes can be further classified as warm or cold, with lake temperatures at mixis exclusively above or below 4 °C, respectively (Wetzel 2001). This study focuses on a warm monomictic system, Cultus Lake.

Warm monomictic lakes are common in tropical and moderate temperate climates, such as coastal regions that are influenced by oceanic climates (Wetzel 2001; Kalff 2002). Warm monomictic lakes stratify vertically into layers following insolative heating in the spring, a pattern that becomes more intense through the summer, characterized by a warmer, less dense upper layer (epilimnion) overlying a cooler, more dense bottom layer (hypolimnion) (Wetzel 2001). These layers are separated by a region of rapidly changing water temperature with depth, known as a metalimnion, which contains the thermocline, defined as the plane of maximum rate of decrease of water temperature with respect to depth (Wetzel 2001).

Once seasonal stratification is established, the epilimnion is exposed to the atmosphere where oxygen can be dissolved into the water surface

by diffusion. The epilimnion contains the upper euphotic zone (region of photosynthetically-active light penetration) and is associated with autotrophic production by phytoplankton, which adds oxygen and seasonally depletes nutrients from this lake region (Wetzel 2001). The density gradient at the thermocline generally inhibits mixing between the epilimnion and hypolimnion, but not the settling of senescent organic matter. Aerobic decomposition of settling organic matter and internal loading from lake sediments can result in somewhat lower hypolimnetic dissolved oxygen concentrations towards the end of the stratified period, and comparatively higher hypolimnetic nutrient concentrations, the magnitudes of which scale with lake trophic status (Wetzel 2001; Søndergaard et al. 2003).

Thermal stratification typically breaks down in the fall and winter as surface water temperatures cool and wind stresses gradually mix the two layers, ultimately resulting in isothermal conditions and complete vertical mixing of the water column, known as lake turnover (Wetzel 2001). In monomictic systems, this complete mixing is maintained until the spring when solar heating is sufficient to thermally re-stratify the lake. This complete mixing of a lake is necessary to re-oxygenate the hypolimnion while at the same time redistributing hypolimnetic nutrients to the epilimnion for use by primary producers during the growing season.

1.2 Climate Change and Lakes

The direct primary influences of climate change on lake thermal structure are mediated by heat exchanges with the atmosphere via solar radiation, longwave radiation, latent (evaporative) heat, and sensible (convective) heat (Imboden and Wüest 1995). Abiotic and biotic dynamics in lake ecosystems are often tightly coupled with atmospheric processes and relatively small changes in resultant lake temperatures could potentially elicit disproportionately large effects on the physical and ecological characteristics of lakes (Adrian et al. 2009). Thus, any significant changes in climatic forcings of lakes are expected to influence lake dynamics, and potentially be interactive with other lake stressors (Christensen et al. 2006).

Past site-specific studies on lakes (e.g. Sahoo et al. (2015)) and lakes in specific climatic regions (e.g. George et al. (2007)) have demonstrated that climate change is altering the physical characteristics of lakes which has the capacity to alter water quality and affect whole lake ecosystems, including reducing habitat for cold-water fish. Additionally, comprehensive global studies show an increasing trend in lake surface temperatures over recent

decades (O'Reilly et al. 2015) along with air and ocean surface temperatures (IPCC 2013). However, lake surface temperature and air temperature correlations can vary regionally, and warming (or cooling) rates are dependent on local climate and geomorphology (O'Reilly et al. 2015). Thus, there is a need to assess the effects of climate change on lakes on a case-by-case basis.

The thermal structure of lakes is a sensitive indicator of climate change because of their responsiveness to climate forcings (Adrian et al. 2009). Epilimnetic temperatures are an indicator of local climate trends: warming in the water surface increases as air temperature increases (Adrian et al. 2009). Conversely, hypolimnetic temperatures do not necessarily increase with air temperature and may in fact exhibit cooling trends, depending on lake morphometry (Gerten and Adrian 2001; Adrian et al. 2009). Increased warming is predicted to force stronger temperature gradients in lakes, intensifying and prolonging stratification (Ficke et al. 2007; Adrian et al. 2009). Globally, the strength and duration of lake stratification has been increasing in recent decades with the largest increases found in warm, deep lakes (Kraemer et al. 2015). Stronger and prolonged stratification is particularly problematic for warm monomictic lakes, where there is only one mixing season per year, as reductions in thermal exchange, nutrient redistribution, and dissolved oxygen regeneration occur. With sufficient warming, there is a possibility for warm monomictic lakes to shift mixing regimes to oligomixis (i.e. inconsistent annual overturn) or even towards a non-mixing state (meromixis) (Livingstone 2008), thereby limiting exchanges between the epilimnion and hypolimnion. This non-mixing state reduces hypolimnetic dissolved oxygen, and the decomposition of sedimented organic matter can increase hypolimnetic salinity, further inhibiting mixing due to chemically-mediated increases in density and stability, leading to meromixis (Kalff 2002).

Climate change can also elicit complex and often unpredicted lake ecological responses through interactions with a variety of lake and watershed drivers and stressors (Christensen et al. 2006). For instance, climate change is accelerating the rate of natural and cultural eutrophication in lakes (B. Moss et al. 2011). The increased frequency and strength of storms, predicted with climate change, is expected to increase runoff and nutrient loading into lakes (Adrian et al. 2009; Robertson and Rose 2011). Key limiting nutrients, like phosphorus and nitrogen, can come from regions with high industrial, agricultural, residential, or geological sources, while dissolved organic carbon fluxes can increase from runoff in heavily forested regions (Anderson et al. 2002; Schelker et al. 2014; McGinley et al. 2016). The resultant increases in nutrient inputs and changing stoichiometry (i.e. nitrogen to phosphorus

ratio) can lead to algal blooming, and structural and functional changes in algal and reliant zooplankton communities, including increases in problematic algal taxa, such as cyanobacteria (O'Neil et al. 2012) and increased growth rates of invasive plant species (Ficke et al. 2007). Moreover, warmer water temperatures from increased heating may reduce oxygen concentration in lakes (Ficke et al. 2007). Prolonged seasonal lake stratification can enhance organic matter delivery to lake hypolimnia, resulting in accelerated depletion of hypolimnetic dissolved oxygen concentrations (Ficke et al. 2007). Warming hypolimnetic waters reduce the solubility of oxygen, further diminishing deep water dissolved oxygen concentrations (Kalff 2002). Together, increased nutrient loading and warmer water temperatures will significantly change food webs and habitat for fish, likely enhancing fish mortality for many cold-water species, and generally changing fish community composition (Ficke et al. 2007). It is therefore important to study the effects of climate change and eutrophication on lake ecosystems in order to improve watershed planning, and develop mitigation strategies that minimize the impacts on ecosystems and ecosystem services.

1.3 Cultus Lake

Cultus Lake, located in British Columbia's Fraser Valley region, is experiencing increased nutrient loading that is leading to lake eutrophication (Shortreed 2007; Putt 2014; Chiang et al. 2015). Nitrogen and phosphorus are being loaded into the lake from several key sources: wet and dry atmospheric deposition from major urban, industrial, and agricultural centres upwind, upstream agricultural runoff from Columbia Valley and its unconstrained aquifer, septic leaching, and migratory gull guano (Putt 2014). The lake has historically been classified as oligotrophic (Shortreed 2007), but observational data and state-based modelling indicate that increased nutrient loading is transitioning the lake to mesotrophy (Putt 2014). Such fundamental changes in the ecosystem may be increasing threats to two resident species-at-risk for which Cultus Lake is critical habitat: the Cultus Lake Pygmy Sculpin (*Cottus aleuticus*; SARA 2002; COSEWIC 2010) and Sockeye Salmon (*Oncorhynchus nerka*; COSEWIC 2003). As the population of British Columbia's Lower Mainland grows, use of Cultus Lake by humans is expected to increase along with associated anthropogenic nutrient loading.

The climate in the Fraser Valley has been warming since at least 1900, a trend that is projected to continue changing in the future (Pacific Climate Impacts Consortium 2012; British Columbia Ministry of Environment 2016).

The mean air temperature in Southern Coastal regions of British Columbia has increased by + 0.8 °C per century (British Columbia Ministry of Environment 2016). A downscaled ensemble of climate change models under various greenhouse gas emissions scenarios predict an expected mean temperature increase of + 1.0 °C, + 1.8 °C, and + 2.8 °C for the 2020s, 2050s, and 2080s, respectively above a thirty year historical average in 1961–1990 (Pacific Climate Impacts Consortium 2012). Annual precipitation has historically increased by + 14 % per century since at least 1900 (British Columbia Ministry of Environment 2016) and is expected to continue increasing by + 4 %, + 7 %, and + 9 % for the 2020s, 2050s, and 2080s, respectively above the same thirty year baseline with wetter winters and drier summers (Pacific Climate Impacts Consortium 2012). Climate change is therefore expected to significantly affect the thermal characteristics of Cultus Lake as air temperatures increase and the watershed hydrological regime changes.

1.4 Thesis Objectives

Cultus Lake has been studied extensively since the 1920s because of its Sockeye Salmon population (Foerster 1925; Ricker 1937). While more recent studies have focused on nutrient loading (Shortreed 2007; Putt 2014), climatically-forced physical limnological processes are likely to play a role in enhancing the eutrophication of Cultus Lake. This study investigates the following questions in more detail:

1. How are changing physical processes in the lake affecting eutrophication and critical habitat for species-at-risk?

2. How has climate change historically affected physical processes in Cultus Lake?

3. How will Cultus Lake's seasonal patterns of thermal stratification evolve as climate change continues?

These questions are addressed through development and parameterization of a one-dimensional Lagrangian hydrodynamic model (General Lake Model, GLM; Hipsey, Bruce, et al. 2014) calibrated using field data from Cultus Lake. The numerical lake model is coupled with the fourth iteration of the Canadian Regional Climate Model (CanRCM4; Environment and Climate Change Canada 2017) to predict how physical processes in the lake may change in the future through 2100 AD. Additionally, the model is hindcast

to assess how the lake has changed since the 1920s to validate more simplistic state-based models (e.g. BATHTUB; Putt 2014).

Chapter 2

Methods

2.1 Site Description

Cultus Lake is situated in the eastern Fraser Valley, British Columbia, Canada, approximately 95 km east of Vancouver and due south of Chilliwack. The lake is a part of the ancestral territory of the Soowahlie Band of the Stó:lō peoples. The lake is traditionally known by the Stó:lō peoples as *Swí:lhcha* and was the location of the community of The'wá:lí (Trimble 2016). The lake is characterized as a single basin with a length of approximately 5.0 km and a width of 1.5 km. A recent bathymetric survey by the Canadian Hydrographic Service (Section 2.2.3, Figure 2.1) in 2016 resulted in a surface area of 6.3 km^2, a mean depth of 32 m, and a maximum depth of 43 m. Cultus Lake is currently classified as a warm monomictic lake with a long summer stratification period (Shortreed 2007), and has previously been observed to inversely stratify but never for a prolonged period with rare ice coverage (Ricker 1937). The lake is situated in the hanging Columbia Valley above the Chilliwack River at an elevation of 45 m a.s.l., bounded by Vedder Mountain to the west and International Ridge to the east. The total catchment area is 75 km^2 (Shortreed 2007), of which approximately 16 km^2 is located in the United States state of Washington. A municipal park and community is situated on the north shore of the lake and is overseen by the Cultus Lake Park Board. The southern shore of the lake has been developed as the community of Lindell Beach. Both the east and west shores of the lake are within the boundaries of Cultus Lake Provincial Park which extends up the slope of Vedder Mountain and International Ridge toward the United States border. Cultus Lake is a popular recreation site due to its proximity to major urban centres in the Lower Mainland. Between 2 and 3 million people visit Cultus Lake every year with this number projected to grow as population in the Lower Mainland increases (Delcan 2012 as cited by Putt 2014).

The Cultus Lake watershed has 11 major tributaries (Putt 2014), of which the three largest were included in this study to parametrize GLM: Frosst Creek, Watt Creek, and Smith Falls Creek. Inflows were deemed

important for this study because of the short residence time of the lake (1.8 years, Shortreed 2007) and the long time-scale of this study. The outlet, Sweltzer River (sometimes referred to as Sweltzer Creek), drains Cultus Lake northward to the Chilliwack River, a tributary of the Fraser River which drains into the Strait of Georgia at Vancouver, British Columbia. A detailed description of the inflows and outflow is provided in Appendix A.

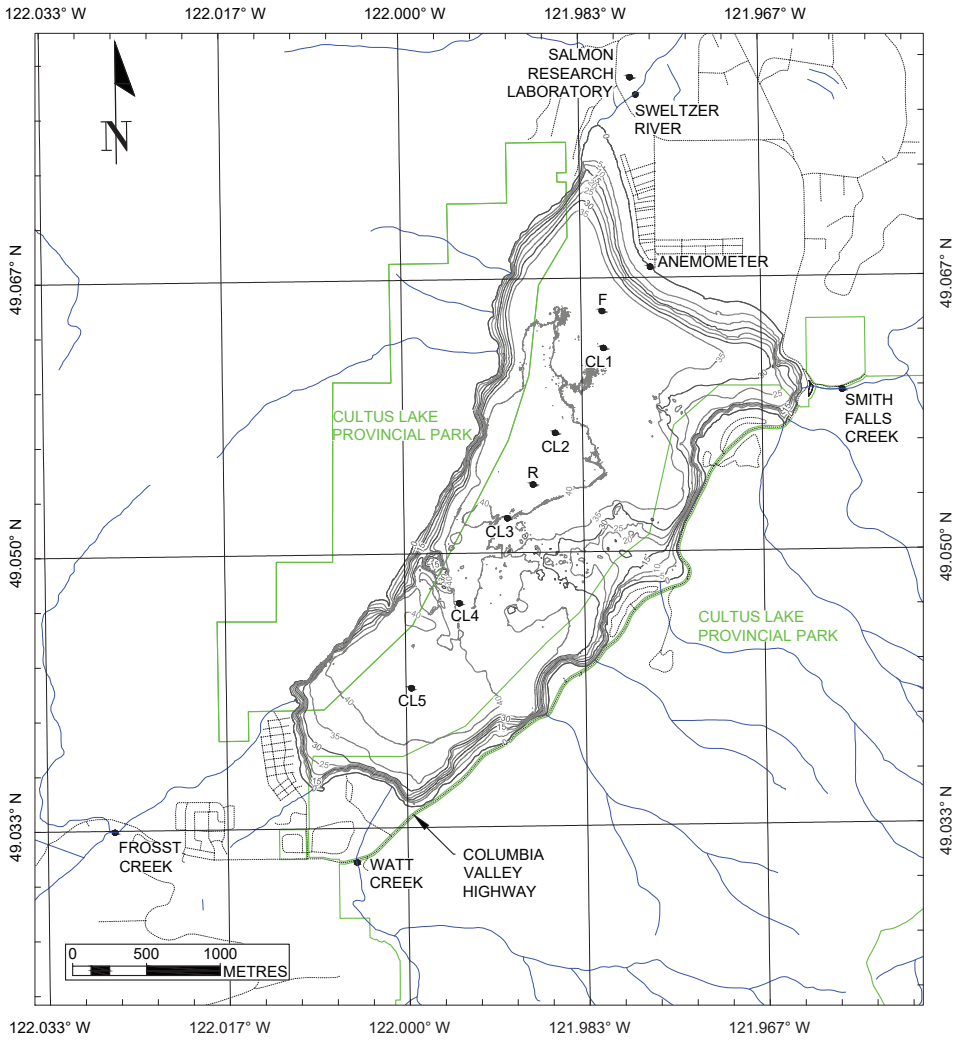

Figure 2.1: Map of Cultus Lake. Bathymetric survey was performed by Canadian Hydrographic Service in UTM Zone 10N with NAD83 Datum. Depths are at 5 m contour intervals. The waterline is estimated at 44.5 metres above sea level. National Hydro Network and National Road Network were obtained from Natural Resources Canada's GeoGratis web-service.

2.2 Data Collection

Various forms of data were collected to evaluate the thermal changes in Cultus Lake with climate change. Historical observations dating to the 1920s were obtained to provide insight into changes in Cultus Lake over the past century. More recent data were used to calibrate and validate (hindcast) GLM which was used to investigate changes to the lake under different warming scenarios projected through 2100.

2.2.1 Historical Data

The first major limnological surveys of Cultus Lake were performed in the 1920s and 1930s to study the propagation of Sockeye Salmon (e.g. Foerster 1925). The historical data are useful to provide insight into how the thermal characteristics of the lake have changed over the past century. Temperature profiles were available from April 1923 through October 1923, and January 1924 near the north end of the lake (marked "F" on Figure 2.1; Foerster 1925). Monthly profiles were taken in June 1927–September 1929 by Dr. Foerster at a "central station" (Ricker 1937); further semi-monthly profiles were taken at a central station (marked "R" on Figure 2.1) January 1932–January 1937 (Ricker 1937). In 1923, temperature measurements were performed using a modified deep-sea thermometer equipped with a one-way valve that let in water on descent. The thermometer was kept at the desired depth for several minutes before being rapidly hauled to the surface (Foerster 1925). For later studies, temperature measurements were performed using a Negretti and Zambra deep-sea reversing thermometer with graduations to 0.2 °C, and readings typically made to the nearest 0.1 °C (Ricker 1937).

Additional historic conductivity, temperature, and depth (CTD) data were provided by Fisheries and Oceans Canada (DFO). Monthly data were collected from 18 April 2001–13 March 2003 and 17 February 2009–present day as part of ongoing limnological surveys. The primary DFO study station is at approximately the same location as station CL2 (Figure 2.1). CTD casts were performed using an Applied Microsystems Ltd. MicroCTD and an Applied Microsystems STD-12 Plus recording at 1 Hz.

2.2.2 Meteorological Data

Meteorological data were collected from several locations near Cultus Lake. An Onset HOBO H21 weather station was installed on the roof of the Cultus

Lake Marina at the northeast end of the lake on 12 August 2016 (Figure 2.1). This site was chosen to minimize tampering while also capturing wind speeds along the lake's long-axis. The weather station was equipped with an Onset barometric pressure sensor and anemometer set to measure the 10-minute average pressure [mbar], and wind speed [$\mathrm{m\,s^{-1}}$] and wind direction [degrees from North]. Table 2.1 provides the accuracy, resolution, and drift of the weather station components. The elevation of the anemometer was estimated to be 5 m above the ground so a correction to 10 m was required assuming a log profile:

$$U_{10} = U_z \frac{\ln\left(\frac{10}{z_0}\right)}{\ln\left(\frac{z}{z_0}\right)} \tag{2.1}$$

where U_{10} is the wind speed at 10 m, U_z is the observed wind speed at height z, and z_0 is the aerodynamic roughness length (Wieringa 1992). For winds between 140° and 310°, a roughness length of 0.005 m was assumed for the smooth lake surface. Between 310° and 140°, a roughness of 2.0 m, described as 'chaotic', was assumed due to the irregular topography and the height of the surrounding trees. Due to the relatively late installation of the weather station in the study, correlations of wind speed were required for nearby Environment Canada reporting stations. Wind speed measurements obtained at the marina provided insight into the dominant wind directions and to determine the best fit for historical wind data and to fill in the missing dataset. No strong correlations were found for wind speeds between Cultus Lake and nearby weather stations. However, it was determined that wind speeds reported at the Abbotsford International Airport (49.025°N 122.360°W, Elevation: 59.1 m, Climate ID: 1100030 & 1100031, WMO ID: 71108, ICAO: CYXX) provided the best fit, though were slightly stronger than those measured at the lake. Barometric pressure obtained at the marina was used to develop a linear trend with nearby weather stations. A strong correlation was found with the barometric pressure measured at Agriculture Canada's Agassiz Research and Development Centre (49.243°N 121.760°W, Elevation: 19.3 m, Climate ID: 1100119, WMO ID: 71113).

Table 2.1: Accuracy, resolution, and drift of HOBO weather station instruments (Onset Computer Corporation 2008, 2017a)

Instrument	Measurement	Accuracy	Resolution	Drift
S-BPA-CM10	Barometric pressure [mbar]	Maximum ± 5	0.1	Typical 1 per year
S-WCA-M003	Wind speed/gust [$m\,s^{-1}$]	± 0.5 ± 3 % 17–30 $m\,s^{-1}$ ± 4 % 30–44 $m\,s^{-1}$	0.19	N/A
	Wind direction [degrees]	± 5	1.4	N/A

Hourly temperature [°C] and relative humidity [%] were obtained from the Environment Canada weather station located at the Cultus Lake Salmon Research Laboratory (49.079°N 121.979°W, Elevation: 45.7 m, Climate ID: 1102221). Total daily precipitation [mm] was obtained from the Abbotsford station. This measurement includes both rain and snow, where 1 cm of snow is equivalent to 1 mm of rain. Cloud cover fraction was obtained from the Abbotsford International Airport Meteorological Terminal Aviation Routine Weather Reports (METARs). Three letter METAR abbreviations for cloud cover were converted to oktas, or eighths of the sky that is occupied by clouds, where CLR = 0, FEW = 2, SCT = 4, BKN = 6, OVC = 8 oktas. METARs report cloud cover with increasing altitude, so the maximum value was obtained for each measurement. Finally, hourly photosynthetically active radiation (PAR [$mol\,m^{-2}\,s^{-1}$]) obtained at the Cultus Lake Laboratory was provided by DFO. Incident shortwave radiation [$W\,m^{-2}$] was calculated from PAR by dividing by 2.11 (Kalff 2002). Gaps in the shortwave radiation data where the sensor malfunctioned were filled with the clear-sky model described by Bird and Hulstrom (1981) and multiplied by a cloud factor of $(1 - 0.65C^2)$, where C is the relative cloud cover of sky (Barry and Chorley 1976). Atmospheric parameters used in the clear-sky model are shown in Table 2.2.

Some historical meteorological data were obtained from different stations than those described above. Temperature and relative humidity data prior to 5 June 2012 (commissioning date of the Cultus Lake station) was obtained from the Abbotsford Airport station. The air temperature correlation between Abbotsford and Cultus Lake is given by $T_{Cultus} = 1.034T_{Abbotsford} -$

Table 2.2: Bird clear-sky model atmospheric parameters

Parameter	Value	Source
Atmospheric pressure	1009 mbar	Average from Onset weather station
Ozone concentration	0.242 atm-cm	3-year average 52 ppb concentration measured at Chilliwack air quality monitoring station (Environmental Reporting BC 2015) integrated over the 10 km troposphere
Aerosol optical depth at 500 nm	0.094	2009–2014 average at Saturna Island (48.783°N 123.133°W; AERONET 2017)
Aerosol optical depth at 380 nm	0.129	2009–2014 average at Saturna Island (48.783°N 123.133°W; AERONET 2017)
Surface albedo	0.2	(Bird and Hulstrom 1981)
Precipitable water mass	1.26 atm-cm	2009–2014 average at Saturna Island (48.783°N 123.133°W; AERONET 2017)

0.792 with a coefficient of determination, r^2, of 0.960. The correlation of the relative humidity data at Abbotsford to Cultus Lake is approximately one-to-one. Additionally, a weather station located in Chilliwack (49.172°N 121.925°W, Elevation: 11.0 m, Climate ID: 11015300) was used for total daily precipitation values, because of its proximity to Cultus Lake, before it was decommissioned after August 2014. Hourly solar radiation and cloud cover were measured at Abbotsford Airport between 1953–2005 and sourced from Environment Canada's Canadian Weather Energy and Engineering Datasets (CWEEDS; Environment and Natural Resources Canada 2017).

2.2.3 Limnological Data

Water temperature data were collected beginning 28 April 2016 at five stations in the lake (Figure 2.1, Table 2.3). The stations were set along the long-axis of the lake with a spacing of 660 m. Both high resolution temporal and spatial temperature data were obtained. High resolution temporal data were collected by installing subsurface moorings of thermistor chains equipped with Onset HOBO TidbiT v2 water temperature sensors

(UTBI-001, ± 0.21 °C accuracy, 0.02 °C resolution, 0.1 °C per year drift; Onset Computer Corporation 2017c) at 4 m depth intervals and logging at 15 minute intervals at stations CL1, CL3, and CL5. The moorings at stations CL3 and CL5 were installed on 28 April 2016, while the third mooring at CL1 was installed on 25 July 2016. The mooring at station CL3 was disturbed by a recreational boater on 5 June 2016 and redeployed by DFO to a nearby location. This mooring was then returned to its original location on 17 June 2016 after reducing the distance between the top two thermistors by 2 m to shorten the line to reduce tampering. All three moorings were retrieved and redeployed on 9 May 2017.

Table 2.3: CTD cast and thermistor mooring station information

Station	Location	Mooring Deployment	Mooring Retrieval
CL1	49.062°N 121.981°W	25 July 2016	9 May 2017
CL2	49.057°N 121.986°W	N/A	N/A
CL3	49.052°N 121.990°W	28 April 2016	9 May 2017[1]
CL4	49.047°N 121.995°W	N/A	N/A
CL5	49.042°N 122.000°W	28 April 2016	9 May 2017

[1] Station CL3 mooring was removed by a boater on 5 June 2016 and was redeployed by DFO to 49.053°N 121.989°W. Mooring was returned to Station CL3 on 17 June 2016.

Higher resolution spatial data were collected at semi-monthly intervals by performing conductivity, temperature, and depth (CTD) casts beginning 20 May 2016 and continuing through 8 December 2016 at stations CL1–CL5 with a Seabird SBE 19plus v2 SeaCAT Profiler (Table 2.4). Additional sensors were equipped on the unit: a WET Labs ECO fluorometer (to provide chlorophyll-a readings), a Satlantic PAR sensor, and a Sea-Point turbidity sensor. Additional CTD casts were performed at the five stations on 28 April 2016 and 5 May 2016 with DFO's Applied Microsystems Ltd. MicroCTD. Vertical profiles were captured by lowering the CTD unit at a rate of 0.5 $\mathrm{m\,s^{-1}}$ while recording at 4 Hz for the Seabird unit and 1 Hz for the DFO unit. The Seabird CTD unit was turned on prior to the casts to obtain a 30 second average barometric pressure correction factor that was applied in post-processing. The data were processed in MATLAB using the Gibbs-SeaWater (GSW) Oceanographic Toolbox v3.05 containing the Thermodynamic Equation of Seawater 2010 (TEOS-10) functions which assumes the chemical composition of seawater (IOC 2010). The GSW toolbox was

used to convert measured conductivity, temperature, and pressure to accurate freshwater depth, salinity, and density values. Data points from each cast were averaged into 1 m layers to reduce minor observational errors. For water temperature, these layers were then spatially averaged across the five stations to calculate an average profile for the entire lake. Additional filtering was performed on the turbidity profiles to remove random spikes in the data: after examining several vertical profiles, it was determined that any turbidity readings greater than 5 FTU in the epilimnion (depth less than 10 m) were anomalous and were removed.

Table 2.4: Accuracy, resolution, and drift for SBE 19plus V2 CTD (Seabird Scientific 2016a)

Measurement	Accuracy	Resolution	Drift
Temperature [°C]	±0.005	0.0001	0.0002 per month
Conductivity [$S\,m^{-1}$]	±0.0005	0.00001 (freshwater)	0.0003 per month
Pressure	±0.1 % of full scale range	0.002 % of full scale range	0.1 % of full scale range per year

Bathymetric data were obtained from a Canadian Hydrographic Service acoustic survey performed on Cultus Lake in 2016 using a 2 m grid spacing. AutoCAD Civil 3D was used to create a contour map (Figure 2.1). A stage-storage calculation was performed in AutoCAD Civil 3D at 1 m vertical intervals to create a hypsograph (Figure 2.2). The water level in Cultus Lake is controlled by means of stop logs to ensure a fairly constant water level throughout the summer months when precipitation is low. The water elevation has historically remained between 44 m and 45 m a.s.l. The average water elevations was assumed to be 44.5 m based on the 2016 water level data provided by the Cultus Lake Park Board (Figure 2.3), which results in a standardized maximum lake depth of 42.5 m.

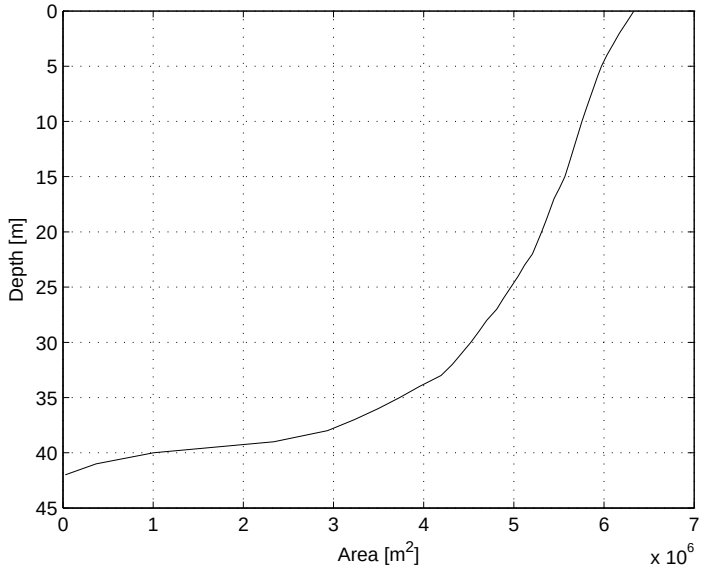

Figure 2.2: Hypsographic curve for Cultus Lake from 1 m stage-storage intervals.

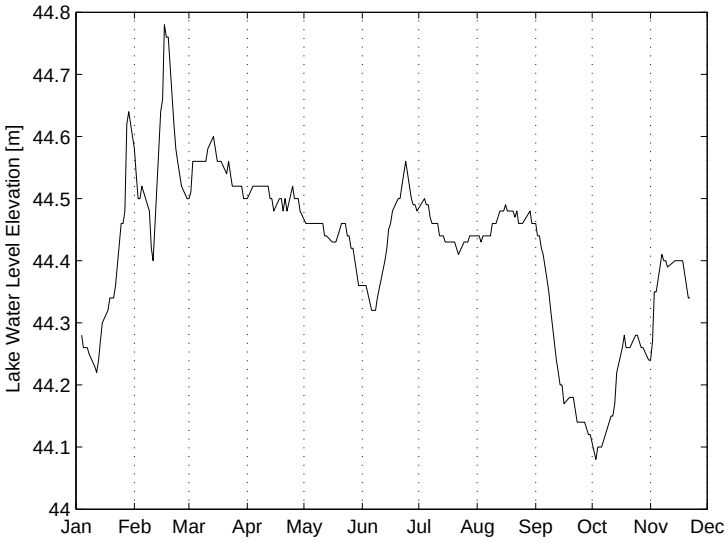

Figure 2.3: Cultus Lake water levels for 2016. Data provided by the Cultus Lake Park Board is in metres above sea-level.

2.2.4 Water Clarity and Extinction Coefficient

Light penetration into the water column is an important driver for shortwave radiation flux and the total available energy for photosynthesis (Kalff 2002). Light penetration decays with depth following the Beer-Lambert Law:

$$I_z = I_0 e^{-kz} \tag{2.2}$$

where I_z is the irradiance [$\mu mol\, m^{-2}\, s^{-1}$] at depth z [m], I_0 is the irradiance just below the water surface, and k is light extinction coefficient [m^{-1}]. The light extinction coefficient can therefore be calculated from the slope of $-ln(I_z/I_0)$ with depth z. The 1 m averaged PAR profile from each semi-monthly excursion was used to calculate k. This calculation has been limited to the euphotic zone which can be defined as the region that receives greater than one percent of the surface light penetration (Kalff 2002). The surface incident light was taken as the value in the second layer due to a 0.6 m offset between the pressure sensor and PAR sensor. To complement this method of calculating k, a Secchi depth measurement was taken from the shaded side of the vessel at station CL2 to coincide with DFO measurements. The light extinction coefficient can be calculated by dividing the measured Secchi depth by 1.7 (Kalff 2002).

2.2.5 Inflows and Outflow

Three inflows for Cultus Lake were regularly measured for discharge, temperature, conductivity, and turbidity. The three largest inflows by drainage area were determined from Putt (2014): Frosst Creek, Watt Creek, and Smith Falls Creek. Gauging station location and drainage area information are provided in Table 2.5. Temperature, conductivity, and turbidity were measured using the Seabird CTD initially on 17 June 2016 and semi-monthly beginning 25 July 2016 until 16 November 2016. Semi-monthly discharges were measured in the three inflows using a Swoffer 3000 flow meter (3 % accuracy; Instruments 2016) beginning 25 July 2016 until 16 November 2016. A HOBO TidBiT v2 logger was installed in Frosst Creek on 17 June 2016 just upstream of the Columbia Valley Highway to measure water temperatures every 10 minutes alongside a HOBO water level logger (U20-001-01; Pressure: $\pm$0.3 % accuracy, <0.02 kPa resolution, <0.3 % stability; Temperature: $\pm$0.44 °C accuracy, 0.1 °C resolution, 0.1 °C stability (Onset Computer Corporation 2017b)) that measured water pressure at 10 minute intervals. The water pressure measured by the logger was barometrically adjusted using the corrected pressure measured at Agassiz and

the onshore weather station. This adjustment was used to calculated water depth which was used to obtain values for discharge based on a rating curve developed from measurements obtained by Putt (2014), assuming a power rating curve equation (ISO 2010):

$$Q = \beta(h - h_0)^{\alpha} \tag{2.3}$$

where Q is the discharge [$m^3 s^{-1}$], h is the stage [m]. β, h_0, and α are calibration coefficients: β is the discharge when $(h - a)$ is 1 m, h_0 is the gauge height when flow is zero, α is the rating curve slope. This equation allows a shift in values for h_0 between locations, assuming the creek has the same cross-sectional shape at those locations. Since pressure loggers were not installed on Smith Falls and Watt Creeks, rating curves for those creeks were not created, and a linear trend was assumed between discharge measurements. As a result, instantaneous discharges were not obtained for Smith Falls and Watt Creeks for 2016. Instantaneous discharges for these three inflows for 2011–2013 were obtained from Putt (2014).

Table 2.5: Stream gauging station information

Stream Name	Location	Drainage Area [km^2]
Frosst Creek	49.033°N 122.027°W	36.3 (Water Survey of Canada Station 08MH072)
Watt Creek	49.031°N 122.005°W	6.58 (Putt 2014)
Smith Falls Creek	49.060°N 121.959°W	6.49 (Putt 2014)
Sweltzer River	49.078°N 121.978°W	75.0 (Shortreed 2007)

A linear regression was established between the air temperature and creek temperatures of the form:

$$T_s = aT_a + b \tag{2.4}$$

where T_s is the stream temperature [°C], T_a is the air temperature [°C], and a and b are stream specific coefficients. Table 2.6 provides the calculated coefficient values. This correlation was used to determine the daily average creek temperature for Watt and Smith Falls creeks rather than interpolating between stream temperature measurements. For Frosst Creek, the hourly average stream temperature from the HOBO TidBiT was used to correlate with the hourly air temperature. The temperature of the smaller watercourses (Watt Creek and Smith Falls Creek) have higher r^2 values

than Frosst Creek because of their stronger response to changes in air temperature from a smaller thermal inertia (Stefan and Preud'homme 1993). Turbidity and salinity values derived from the CTD data in each creek were linearly interpolated between measurements.

Table 2.6: Stream temperature coefficients for Equation 2.4

Stream Name	a	b	r^2
Frosst Creek	0.167	6.885	0.629
Watt Creek	0.422	3.626	0.885
Smith Falls Creek	0.344	6.395	0.905

Outflow data on Sweltzer River were obtained by installing a HOBO water level logger (U20-001-01) recording at 10-minute intervals on 5 October 2016 downstream of the fish counting fence outside the Salmon Research Laboratory and barometrically adjusting the water pressure to obtain depth. Flow measurements were obtained on 5 October 2016 and 8 December 2016 to adjust a power rating curve fitted to data from Putt (2014). DFO provided daily staff gauge readings and temperature for the period of 11 July 2016–20 October 2016, which were also adjusted to the rating curve. However, the staff gauge is located upstream of the fish counting fence, thus the conversion between readings and discharge is only applicable when sections of the fence are open because the closed fence acts as a weir.

2.3 General Lake Model (GLM)

Cultus Lake was modelled using the open-source one-dimensional Lagrangian hydrodynamic General Lake Model (GLM, v2.2β) developed by the Aquatic EcoDynamics Research Group at the University of Western Australia (Hipsey, Bruce, et al. 2014). GLM is used to simulate long-term changes in the vertical distribution of temperature, salinity, and density by accounting for the effects of surface heating and cooling, and inflows and outflows. The model can be coupled with the Aquatic EcoDynamics library (AED) to simulate lake biogeochemistry; however, AED was not incorporated in this study.

2.3.1 Model Description

GLM follows a Lagrangian structure with homogeneous layers that can contract and expand from changes in the layer density due to surface heating,

vertical mixing, inflows, and outflows. Layers are sorted by stability according to density and with varying thicknesses to resolve the density gradient. The density of each layer is computed at each timestep based on temperature and salinity from the equation of state described in UNESCO (1981). Maximum and minimum layer thicknesses are set by the user; the maximum thickness should be at least twice the minimum thickness to ensure proper layer merging. The primary drivers for the model, and changes in layer density, are from meteorological forcings that alter the water temperature.

Surface boundary layer fluxes provide energy for heating and mixing the lake. The driving fluxes are shortwave radiation, longwave radiation, and sensible (convective) and latent (evaporative) heat fluxes. Solar radiation is the primary driver for lake thermodynamics. Solar radiation data may be specified directly or GLM can calculate the theoretical surface irradiance based on the clear-sky model from Bird and Hulstrom (1981) which can be corrected for cloud cover, if available. The reflected fraction of shortwave radiation is dependent on the lake albedo. Several options for the calculation of albedo are given for the user (see Hipsey, Bruce, et al. 2014). Shortwave radiation penetrates into the lake following the Beer-Lambert Law (Equation 2.2). The Beer-Lambert Law is only applied to the PAR fraction (45 % in GLM) of incident light, while the surface layer accounts for all incident light that is not reflected. Longwave radiation can be specified as a net flux, incoming flux, or an incoming flux computed based on cloud cover fraction and air temperature. Several options described in Hipsey, Bruce, et al. (2014) are provided to calculate longwave emissivity accounting for reflection from clouds. If no longwave radiation data are available, the model will approximate the cloud fraction from solar irradiance. Sensible and latent heat fluxes are calculated from common bulk aerodynamic formulae. The sensible heat flux is dependent on wind speeds and air temperatures, while the latent heat flux is most strongly dependent on wind speeds. The sensible and latent heat fluxes account for a minor portion of the net heat flux and can vary greatly day-to-day depending on wind speeds.

Surface mixing in GLM is accomplished by comparing the available energy and required energy to undergo mixing at each time-step. The balance between the turbulent kinetic energy (TKE) and the required energy to undergo mixing (potential energy) provides the surface mixed layer deepening rate. Wind stirring, convective overturning, and Kelvin-Helmholtz (K-H) billowing contribute to the TKE, while the potential energy is the energy required to lift up water at the bottom of the mixed layer and accelerated it to the mixed layer velocity in addition to energy dissipated in K-H production (Hipsey, Bruce, et al. 2014). The premise for the model's algorithm is

described in Imberger and Patterson (1981); a complete outline for surface mixing is available in Hipsey, Bruce, et al. (2014).

The layers are subject to a mass balance at the end of each day that are dependant on evaporation, precipitation, inflows, and outflows. Layer volumes are calculated from the layer thickness and interpolated areas from the user-defined hypsographic curve. Evaporation and precipitation only occur in the surface layer, but all layers are subject to mass conservation from inflows and outflows. Both surface runoff and submerged inflows (e.g. groundwater) can be simulated. For surface inflows, the inflow intrudes the model layers and entrains water from them until the inflow reaches a neutral buoyancy, where a new layer is formed. The rate of entrainment is adapted from Fisher et al. (1979). The user specifies the stream half-angle and the incoming slope. Submerged inflows are inserted at a user specified depth and have no entrainment, but instead mix with adjacent layers until a neutral buoyancy is reached. Three types of withdrawals may be specified: outflows, seepage, and overflow. Withdrawals are all calculated from a similar algorithm; however, a depth must be specified for outflows, whereas seepage is removed from the bottom layer, and overflow is the volume of water in excess of maximum storage.

2.3.2 Model Setup

The physical model is configured in a text file split into several blocks:

- glm_setup: general simulation information including number of layers, maximum and minimum layer thickness, minimum layer volume, light extinction coefficient, and mixing parameters
- morphometry: lake latitude and longitude, basin length and width, and bathymetry input as a hypsograph.
- time: simulation start and stop times, timestep, and time zone
- output: output file details for depth specific outputs and bulk file, daily lake heat flux and water balance summary file, outlet and overflow output file specifications
- init_profiles: initial values of depth, temperature, and salinity.
- meteorology: information on surface forcing and meteorology data. Options for calculating albedo and emissivity are specified. A separate text file containing data for shortwave radiation, cloud cover, air

temperature, relative humidity, wind speed, daily rainfall. Sub-daily values can be provided, except for rainfall because the mass balance occurs only once per day.

- inflows: inflow morphometry consisting of the streambed half-angle, slope, and drag. Inflow data for each inflow are provided in its own file consisting of daily discharge, stream temperature, and stream salinity.

- outflows: outlet elevation, basin length and width at outlet. Similarly to inflows, outflow discharge for each outflow is provided in its own file. Outflow temperature is calculated by the model depending on the elevation of the outlet.

GLM was run for several periods to simulate the thermal characteristics of Cultus Lake: a calibration in 2016, a validation in 2009–2016, a second validation and climate model evaluation in 2001–2003, and two forecast scenarios for 2009–2100. The initial model calibration was completed using the semi-monthly field data obtained in 2016. Because GLM is a one-dimensional model, spatially averaged thermal profiles were used for model evaluation. Lake conditions from 28 April 2016 at 17:00 PST were used as the initial profile. Both temperature and salinity were included in the model for the calibration period, but only thermal profiles were used to evaluate the model. The model was run at an hourly timestep until 12 December 2016 at 12:00 PST and data from every timestep was saved. Only thermal profiles from a single station were available for the 2001–2003 and 2009–2016 periods, so the initial salinity was assumed to be the same as the observations in 2016. The model was run at an hourly timestep from 17 February 2009 12:00 to 8 December 2016 12:00. A daily profile at noon was saved for model validation. For the 2001–2003 hindcasts, the model was initialized at 18 April 2001 12:00 and run hourly until 14 March 2003 12:00. Again, only a daily profile was saved to file. Finally, for the 2009–2100 forecasts, the model was run at an hourly timestep, and only a daily profile was saved. The forecast simulations were initialized at 17 February 2009 12:00. The regional climate forecast data are only available at a daily timestep (Section 2.4), but because the model was calibrated and validated using hourly meteorological data, the model forecast scenarios were run at an hourly timestep using daily average data. However, to prevent excess heating from shortwave radiation, the model automatically assumes an idealized diurnal cycle based on the daily average shortwave radiation (Hipsey, Bruce, et al. 2014).

2.4 Regional Climate Model

GLM was coupled with the fourth generation Canadian Regional Climate Model (CanRCM4; Environment and Climate Change Canada 2017) to forecast the effects of climate change on Cultus Lake. A regional climate model was used because it reduces the need for bias correction to regional climates such as Cultus Lake. CanRCM4 employs the same physics and setup as the second generation Canadian Earth System Model (CanESM2) but downscaled to a 0.22° horizontal grid (Scinocca et al. 2016). CanESM2 employs an atmospheric-ocean general circulation model, a land-vegetation model, and terrestrial and oceanic carbon cycling. The first generation model is described in Christian et al. (2010) with updates to the second generation described in Arora et al. (2011). CanESM2 was used as the Canadian contribution for the Intergovernmental Panel on Climate Change Fifth Assessment Report (AR5) as part of the fifth phase of the Coupled Model Intercomparison Project (K. E. Taylor et al. 2012; Flato et al. 2013). A result of AR5 was the development of new climate change scenarios called Representative Concentration Pathways (RCP). The four RCPs in increasing severity are RCP2.6, RCP4.5, RCP6.0, and RCP8.5 named after the radiative forcing values for 2100 above pre-industrial levels (R. H. Moss et al. 2010). For CanRCM4, three experiment scenarios are available: a historical simulation for 1950–2005, and two climate change scenarios RCP4.5 and RCP8.5 for 2006–2100. The historical scenario is used as a control run to evaluate the climate model with observed data (K. E. Taylor et al. 2012). RCP4.5 is a moderate warming scenario with an increase of radiative forcing stabilizing near 4.5 $\mathrm{W\,m^{-2}}$ and an atmospheric CO_2-equivalent concentration of 650 ppm after 2100 (R. H. Moss et al. 2010). RCP8.5 is an extreme warming scenario with an increase of radiative forcing greater than 8.5 $\mathrm{W\,m^{-2}}$ and an atmospheric CO_2-equivalent concentration greater than 1370 ppm in 2100 (R. H. Moss et al. 2010).

2.4.1 Forecast Data

Climate forecast data were obtained from CanRCM4 for the grid point nearest Cultus Lake located 10 km to the south. (48.960°N 122.000°W, Elevation: 589.75 m). Daily outputs obtained from CanRCM4 were the following: surface temperature [K], surface downwelling shortwave radiation [$\mathrm{W\,m^{-2}}$], total cloud cover [%], precipitation [$\mathrm{kg\,m^{-2}\,s^{-1}}$], near-surface specific humidity [%], pressure at the grid point [Pa], sea level pressure [Pa], eastward and northward near-surface wind [$\mathrm{m\,s^{-1}}$], and total runoff [$\mathrm{kg\,m^{-2}\,s^{-1}}$].

Some minor adjustments were required to optimize the CanRCM4 outputs from the grid point to Cultus Lake. Precipitation and total runoff were converted to $\mathrm{m\,s^{-1}}$ by dividing by the density of water ($1000\ \mathrm{kg\,m^{-3}}$); total daily precipitation was calculated by subsequently multiplying by $86400\ \mathrm{s\,d^{-1}}$. East and north components of wind speed were combined using Pythagoras' theorem to obtain values for the daily average wind speed.

Air temperature was adjusted to the elevation of Cultus Lake by the moist adiabatic lapse rate following Stull (2015). First, $\varepsilon = 0.622$ [unitless] is the ratio of the molecular weight of moist air to the molecular weight of dry air. The saturated vapour pressure, e_s [kPa], is then calculated from the Clausius-Clayperon equation:

$$e_s = e_0 \exp\left[\frac{L_v}{\Re_v}\left(\frac{1}{T_0} - \frac{1}{T}\right)\right] \tag{2.5}$$

where $e_0 = 0.611$ kPa, $T_0 = 273.15$ K, $\Re_v = 461\ \mathrm{J\,kg^{-1}\,K^{-1}}$ is the gas constant for water vapour, and T is the temperature in Kelvin. L_v is the latent heat of vapourization, which for water is $2.5\mathrm{x}10^6\ \mathrm{J\,kg^{-1}}$. The saturated mixing ratio, r_s [unitless], is calculated from pressure in kPa:

$$r_s = \frac{\varepsilon e_s}{P - e_s} \tag{2.6}$$

Finally the moist adiabatic lapse rate, Γ_s [$\mathrm{K\,m^{-1}}$], is given as:

$$\Gamma_s = \frac{|g|}{C_p}\frac{1 + \frac{r_s L_v}{\Re_d T}}{1 + \frac{L_v^2 r_s \varepsilon}{C_p \Re_d T^2}} \tag{2.7}$$

where g is the gravitational constant, $\Re_d = 0.622\,\Re_v$ is the gas constant for dry air, and the specific heat of air $C_p \approx C_{pd}(1 + 1.84 r_s)$ where the specific heat of dry air, C_{pd}, is assumed to be $1004\ \mathrm{J\,kg^{-1}\,K^{-1}}$. The moist adiabatic lapse rate was then used to adjust the air temperature data from an elevation of 589.75 m to 44.5 m.

Relative humidity was calculated from specific humidity following Stull (2015). First, the air pressure at Cultus Lake, P [kPa], was calculated following the barometric formula using the new air temperature [K]:

$$P = P_0 \exp\left(\frac{-0.0342 z}{T}\right) \tag{2.8}$$

The sea level pressure [kPa] was used as P_0 because the elevation and air temperature at Cultus Lake is closer to that at sea level than that at the

grid point. A new value for e_s was calculated for Cultus Lake from Equation 2.5 using the adjusted temperature. The water vapour pressure, e [kPa], at Cultus Lake was calculated from the adjusted pressure and the specific humidity, q, assuming no change in specific humidity with altitude:

$$e = \frac{qP}{\varepsilon + (1 - \varepsilon)q} \tag{2.9}$$

Finally the relative humidity [%] is given as:

$$RH = 100\frac{e}{e_s} \tag{2.10}$$

Chapter 3

Results

Results from the 28 April 2016–8 December 2016 field campaign are presented in this chapter along with results of the GLM simulations. The field data include the limnological data obtained from the thermistor moorings and the semi-monthly CTD casts, specifically the temperature and conductivity, and results relating to water clarity (light penetration, turbidity, and chlorophyll-a). The inflow data from Frosst Creek, Watt Creek, and Smith Falls Creek are described in addition to the outflow data from Sweltzer River. The Cultus Lake specific tuning of GLM is outlined and evaluated to the 2016 field data. Two hindcast scenarios are presented: the first from 2009–2016 to validate the 2016 model calibration, and the second from 2001–2003 to evaluate climate change data that will be used to forecast the model. Historical thermal data dating to 1923 are compared to more recent data (2001–2003 and 2009–2016) to evaluate changes in heat content and the stratification season. These historical data are also compared to projections in the forecast model to 2100 AD.

3.1 Temperature

High temporal resolution temperature data were obtained from a set of thermistor moorings installed at three locations in the lake, while high spatial resolution temperature data were obtained from semi-monthly CTD casts at five locations in the lake; the results are shown in Figures 3.2 and 3.1a, respectively. The lake was already stratified on the first date of the field campaign (28 April 2016). The surface temperature was initially above 13 °C, while the hypolimnion temperature was near 6.5 °C. The thermocline, defined here as the plane of maximum decrease in temperature (Wetzel 2001), was initially at a depth of 8 m. The surface temperature rose at a steady rate throughout the summer. A strong heating period was observed in mid-June at the same time as the development of a secondary thermocline. Secondary thermoclines occur during days with high surface heating by radiation and when winds are insufficient to mix this warm water with the cooler water below, and can persist for many days if wind energy remains low (Lewis 1979).

The secondary thermocline is shown by a divergence in temperatures of the upper two thermistors on moorings CL3 and CL5: the surface thermistors (2.2 m and 2.7 m at CL3 and CL5, respectively) recorded temperatures of 21 °C, but the second shallowest thermistors (6.2 m and 5.5 m at CL3 and CL5, respectively) did not record this sharp increase in temperature. After June, the epilimnetic thermistors heated in tandem indicating the lake surface layer was well mixed. A maximum surface temperature of 22 °C was observed in late August. The thermocline continued to deepen throughout the summer to a depth of 13 m by 5 October 2016. The thermistors at 10.6, 10.2, and 9.5 m for stations CL1, CL3, and CL5, respectively measured a high temperature variability because these thermistors were located near the thermocline. In the fall, temperatures began to decline in the epilimnion and homogenize as wind began to mix the lake. Sudden increases in temperature at mid-depth in October occured as the warm upper layers mix downwards. The lake finally became de-stratified on 8 December 2016 which was the same day that de-stratification was observed with CTD casts. The lake remained relatively isothermal throughout the winter. In late January 2017, surface temperatures cooled to below 3.5 °C while temperatures at depth remained slightly below 4 °C, and the lake briefly inversely stratified. In mid-February, the lake was isothermal at roughly 2.7 °C. Ice rarely forms on Cultus Lake because air temperatures generally remain at or above 0 °C; the water surface therefore remains open for wind to continue mixing the lake at cooler temperatures which reduces the mixed lake temperature to below the temperature of maximum density without inversely stratifying. Finally, increased warming in the spring caused the lake to stratify in April 2017. Remarkably, the hypolimnetic temperatures recorded in April and May 2017 are roughly 1 °C cooler than hypolimnetic temperatures observed in April and May 2016. The cooler hypolimnetic temperatures may be caused by increased cooling in the winter of 2016–2017 relative to the year before.

Strong wind events dominated along the long-axis of Cultus lake causes high spatial variability due to internal seiching. Higher temperature variability throughout the summer is seen in the upper five thermistors in the off-centre moorings compared to station CL3 (Figure 3.2), which is evidence of seiching. The highest temperature variability is observed near the thermocline where the temperature gradient is largest. A sudden increase in temperature at 14.6 m in Figure 3.2a coincided with a sudden decrease in temperature at 9.5 m in Figure 3.2c on 7 October 2016 at 11:15 a.m. This event also coincided with a sudden brief spike in the outflow discharge in Sweltzer River (Figure 3.4), suggesting a sudden surge of water from the lake. A sudden inflow was not observed by the logger in Frosst Creek; how-

ever, the event occurred at the same time as a large wind event oriented along the long-axis of the lake (220°) with gusts up to 18 $m^3 s^{-1}$ (Figure 3.3). Because the lake was still strongly stratified, there was a large downwelling of warm water at the downwind end of the lake to a depth of at least 14.6 m, along with a large upwelling of cold water at the upwind end of the lake to a depth of at least 9.5 m, and a surge of outflowing water. However, the wind setup was brief and when winds subsided, large internal waves from seiching were not captured by the thermistors. Post event, there was high variability in the thermistor temperatures at mid-depth at CL5 that was not seen in the other moorings. This variability occurred as inflow discharges continue to be elevated, suggesting the cool water from Frosst Creek was plunging.

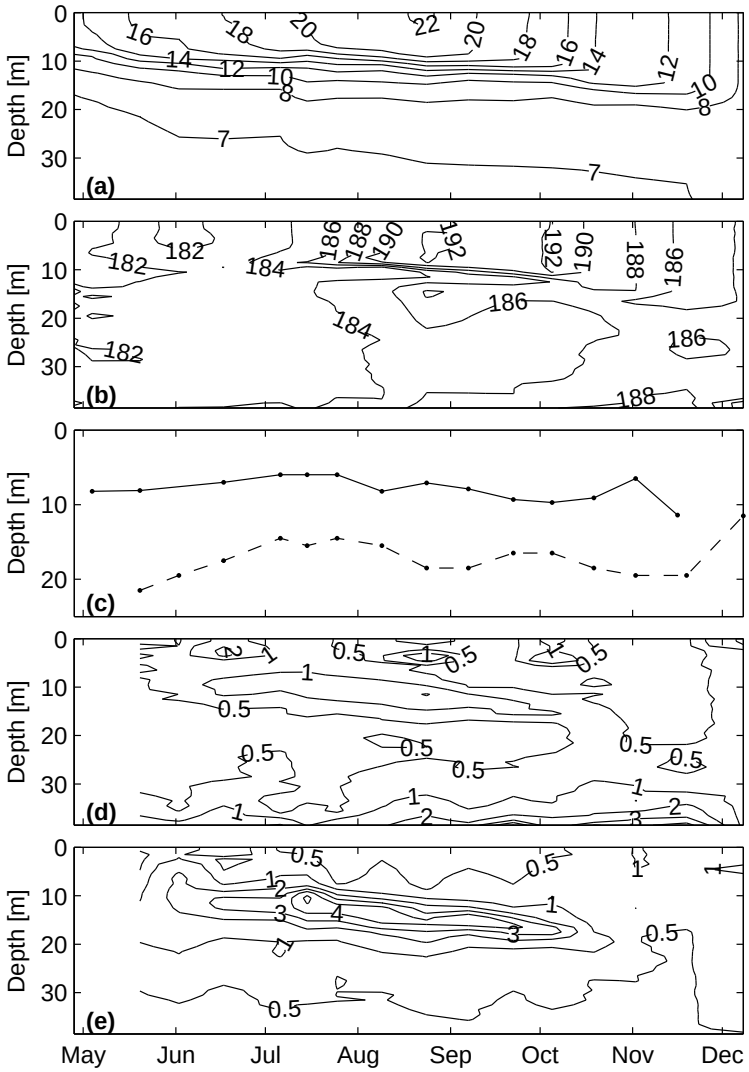

Figure 3.1: Results of limnological field data: (a) water temperature [°C] at station CL3, (b) specific conductivity [$\mu S\,m^{-1}$] at CL3, (c) Secchi depth (solid) at station CL2 and spatially averaged euphotic depth (dashed), calculated from PAR measurements, (e) turbidity [FTU] at CL3, and (f) chlorophyll-a concentration [$mg\,m^{-3}$] at CL3.

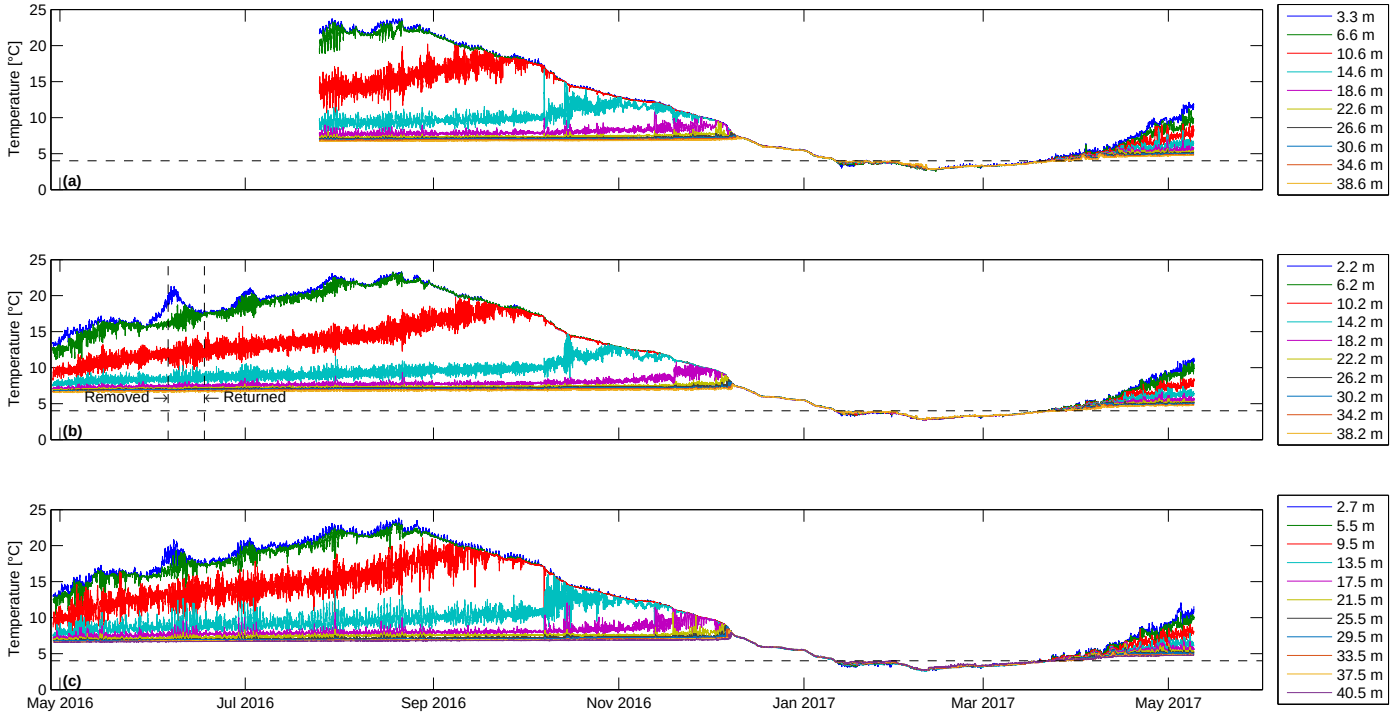

Figure 3.2: Temperature at incremental depths on thermistor moorings CL1 (a), CL3 (b), and CL5 (c). Dashed lines at 4 °C indicate temperature of maximum density. Note: CL3 mooring was repositioned by a boater on 5 June 2016, and returned to the original location on 17 June 2016. Depth of top thermistor in (b) changed from 2.2 m to 4.2 m on 17 June 2016.

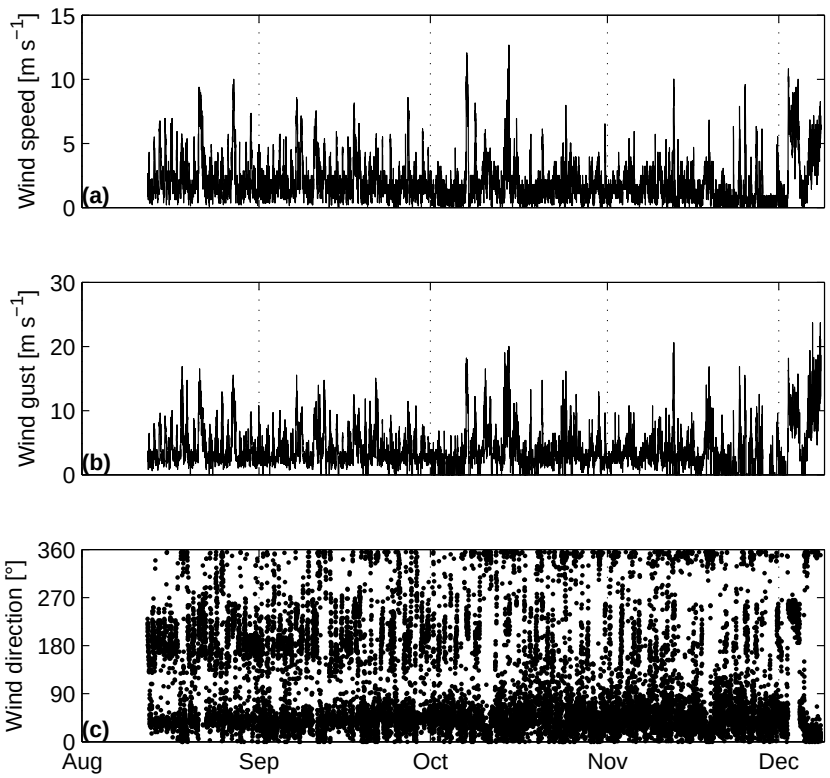

Figure 3.3: 10-minute average wind speed (a), gust (b), and direction (c) at the Cultus Lake Marina.

3.2 Conductivity

Conductivity in Cultus Lake was measured throughout the 2016 field campaign at the five stations using a CTD. Raw conductivity measurements were converted to specific conductivity (conductivity referenced to 25 °C) from the SBE data processing toolbox (Seabird Scientific 2016b):

$$\kappa = \frac{C}{[1 + 0.02(T - 25)]} \tag{3.1}$$

where κ is the specific conductivity [$S\,m^{-1}$], C is the measured conductivity [$S\,m^{-1}$], and T is the measured temperature [°C]. On 5 October 2016, casts were performed at station CL2 with both the Seabird CTD and the MicroCTD to compare results and to determine an offset between data sources. The specific conductivity values calculated from the MicroCTD data were increased by 7.903 $\mu S\,cm^{-1}$ to match the Seabird CTD data; this offset was used for the measurements taken on 28 April 2016 and 4 May 2016. The specific conductivity for the central station, CL3, is shown in Figure 3.1b. The specific conductivity is rather constant at depth in late spring at roughly 182 $\mu S\,cm^{-1}$. The epilimnetic specific conductivity increased to a maximum of 192 $\mu S\,cm^{-1}$ in late August through early October, and began to decrease in the fall to 186 $\mu S\,cm^{-1}$. This epilimnetic increase of conductivity may be caused by atmospheric deposition of ions and particles from air pollutants and sea spray (Wetzel 2001) originating in the Lower Mainland. Another source may be the increase in inflow conductivity in the summer (Section 3.4). The hypolimnetic specific conductivity increased to slightly above 187 $\mu S\,cm^{-1}$ by November. A sharp gradient developed throughout the summer at the thermocline. Conductivity measurements were converted to absolute salinity following the TEOS-10 MATLAB toolbox assuming the lake water has the same chemical composition as seawater. Absolute salinity ranged between 0.081 $g\,L^{-1}$ and 0.091 $g\,L^{-1}$.

3.3 Water Clarity and Chlorophyll-a

Secchi depth measurements were obtained at station CL2 to determine water clarity and light extinction coefficient. The results are shown in Figure 3.1c. The Secchi depth was greater than 8 m in May and decreased into early summer to 6 m. The Secchi depth began to decrease at the beginning of August, and decreased steadily throughout the fall to a depth of 11.4 m on 16 November 2016. It should be noted that high surface waves and heavy rain on 2 November 2016 obscured observations of the Secchi disk. The average Secchi depth over the study period was 8 m. This corresponds to a light extinction coefficient, k, from Equation 2.2 of 0.22 m^{-1} by dividing the average Secchi depth of 8 m by 1.7 (Kalff 2002).

A comparison to the light extinction coefficient obtained from the Secchi depth was performed using PAR data according to Equation 2.2. The euphotic depth roughly follows the trend seen in the Secchi depth (Figure 3.1c). Light penetration on 8 December may have been reduced by high waves affecting the light's angle of incidence and acting as a lens (Dera and Gordon

1968), low angle of the sun's incidence and clouds cover (Reynolds 2009) due to the time of year, and partial obscuration of the sun by mountains to the south along International Ridge. A value for k was calculated for each layer and averaged spatially through the euphotic zone resulting in an average value of 0.23 m^{-1} for the study period, excluding 8 December 2016—similar to k calculated using the Secchi depth.

The turbidity in Cultus Lake was relatively low at 0.5–1.0 FTU. There was an increase in turbidity to above 1.0 FTU near the thermocline in the summer, during the same period as the reduction in Secchi depth (Figure 3.1d) suggesting that the increase in turbidity reduced water clarity. The greatest increase in turbidity occured near the bottom of the lake throughout the summer. A near-benthic turbidity of 1.5 FTU was observed in late May at 40 m, which increased beyond 5.0 FTU in September. This increase is not likely caused by bottom disturbance from the CTD since only the downcast data were analyzed.

Chlorophyll-a is a surrogate for standing algal biomass (Kalff 2002). A clear increase in chlorophyll-a was observed throughout the summer near the thermocline to above 4.0 $mg\,m^{-3}$ (Figure 3.1e). A strong negative correlation was observed between Secchi depth and turbidity, suggesting that biological turbidity from phytoplankton productivity decreased water clarity at metalimnetic depths. Unlike turbidity, chlorophyll-a was not detected in the benthic region of the lake. Presumably, the increase in benthic turbidity was from sedimentation of senescent organic matter (eg. algae and plants) where the chlorophyll-a has broken down to prevent fluorescence.

3.4 Inflows and Outflow

Inflows were monitored beginning 17 June 2016. A water level logger was installed in Frosst Creek to measure the hydrostatic pressure, which was used to calculate the discharge following Equation 2.3 (Figure 3.4). The flow rate remained low throughout the summer near 0.2 $m^3\,s^{-1}$. Stream discharge increased in the fall as rainfall increased, and exhibited a strong response to rainfall. The maximum discharge observed was 5.7 $m^3\,s^{-1}$ on October 8. The discharge remained steady in the fall at approximately 2.0 $m^3\,s^{-1}$. The temperature of Frosst Creek showed a strong diurnal cycle of 2.0 °C in the summer when flows were low. As flows increased in the fall with increased precipitation, the diurnal cycle disappeared as the stream temperature became less responsive to air temperatures because the thermal inertia of the stream increased (Stefan and Preud'homme 1993).

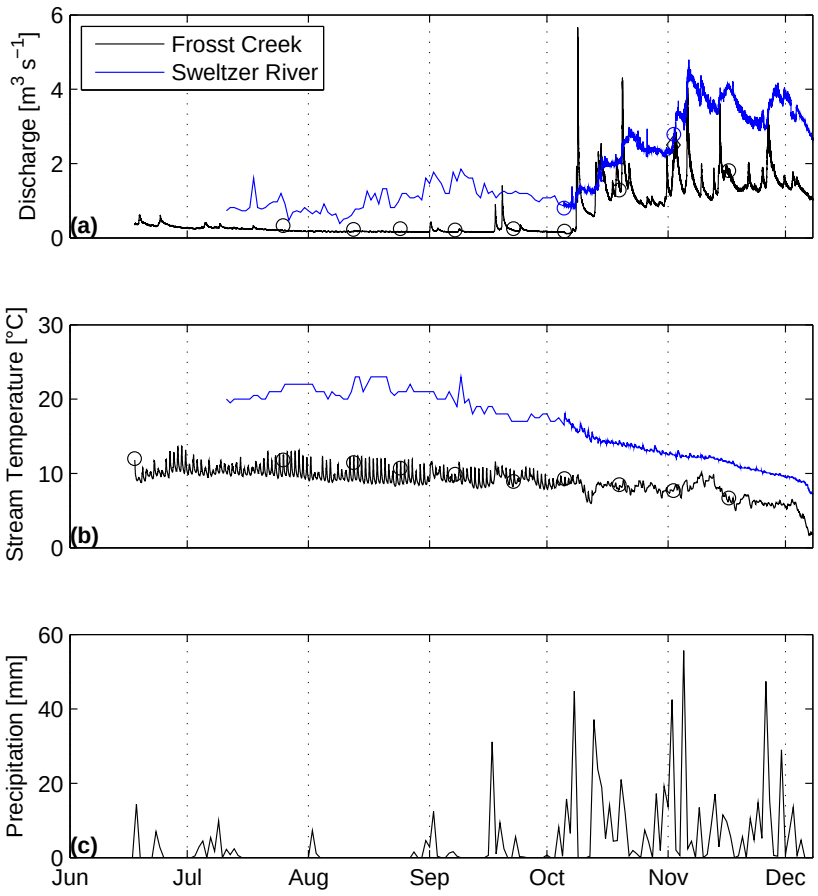

Figure 3.4: 10-minute average discharge derived from rating curve (a) and temperature (b) of Frosst Creek and Sweltzer River, and total daily precipitation (c) at Abbotsford Airport for 17 June 2016 to 8 December 2106. Circles indicate measured values; black diamond on 2 November indicates flow was estimated because stream velocities were too high to safely measure. Daily staff gauge and water temperature readings on Sweltzer River were provided by DFO for dates prior to 5 October 2016.

Stream flow data for the minor tributaries, Watt Creek and Smith Falls Creek are provided in Figure 3.5. The minor tributaries had significantly less flow than Frosst Creek. The flow regime of Watt Creek was found to be intermittent: drying up in the summer and increasing to 0.2 $m^3 s^{-1}$ in the late fall. Smith Falls Creek had a summer baseflow of 0.03 $m^3 s^{-1}$ and also increased to 0.2 $m^3 s^{-1}$ in the late fall. The stream temperatures of Frosst Creek and Watt Creek were relatively similar; both were observed at 12 °C on 17 June and decreasing to 7 °C in November. However, on 25 July, Watt Creek was observed to be 5 °C warmer than Frosst Creek, likely due to the low flow rate being quickly warmed by ambient summer air temperatures. The temperature of Smith Falls Creek was on average 3.6 °C warmer than Frosst Creek throughout the year, with the largest difference on 12 August (6.7 °C). The higher temperature of Smith Falls Creek was possibly caused by warming of extensive wetlands in the upper reaches of this catchment. Specific conductivity followed a similar trend. The average specific conductivity was 204 $\mu S\, m^{-1}$, 194 $\mu S\, m^{-1}$, and 318 $\mu S\, m^{-1}$ for Frosst Creek, Watt Creek, and Smith Falls Creek, respectively. The specific conductivity for Smith Falls Creek was consistently the highest of all three inflows and is consistent with results from Putt (2014). All three inflows saw a decrease in specific conductivity in the fall because of the increase flow rates diluting the water. Increased flows also likely contributed to freshening of the lake in the fall (Section 3.2). Finally, the turbidity in the inflows was 22.4 FTU, 12.6 FTU, and 12.5 FTU for Frosst Creek, Watt Creek, and Smith Falls Creek, respectively. However, a large spike to 103 FTU in Frosst Creek was observed on 25 July of unknown cause and is potentially an anomalous reading. Frosst Creek saw a decrease in turbidity from the summer into the fall, while levels for Watt Creek remained constant relative to 25 July, and Smith Falls Creek saw an increase in turbidity.

Flow rates and temperatures of the outflow, Sweltzer River, are provided in Figure 3.4. Summer discharges ranged between 0.5 $m^3 s^{-1}$ and 1.9 $m^3 s^{-1}$, and summer outflow temperatures ranged between 20 °C and 23 °C. Flow rates increased in the fall as precipitation increased, peaking at 4.8 $m^3 s^{-1}$. Increases in discharge were not responsive to rain events due to the controlling aspect of the lake. Stream temperatures steadily declined in the fall, with a decrease in lake surface temperatures, to a temperature of 7 °C.

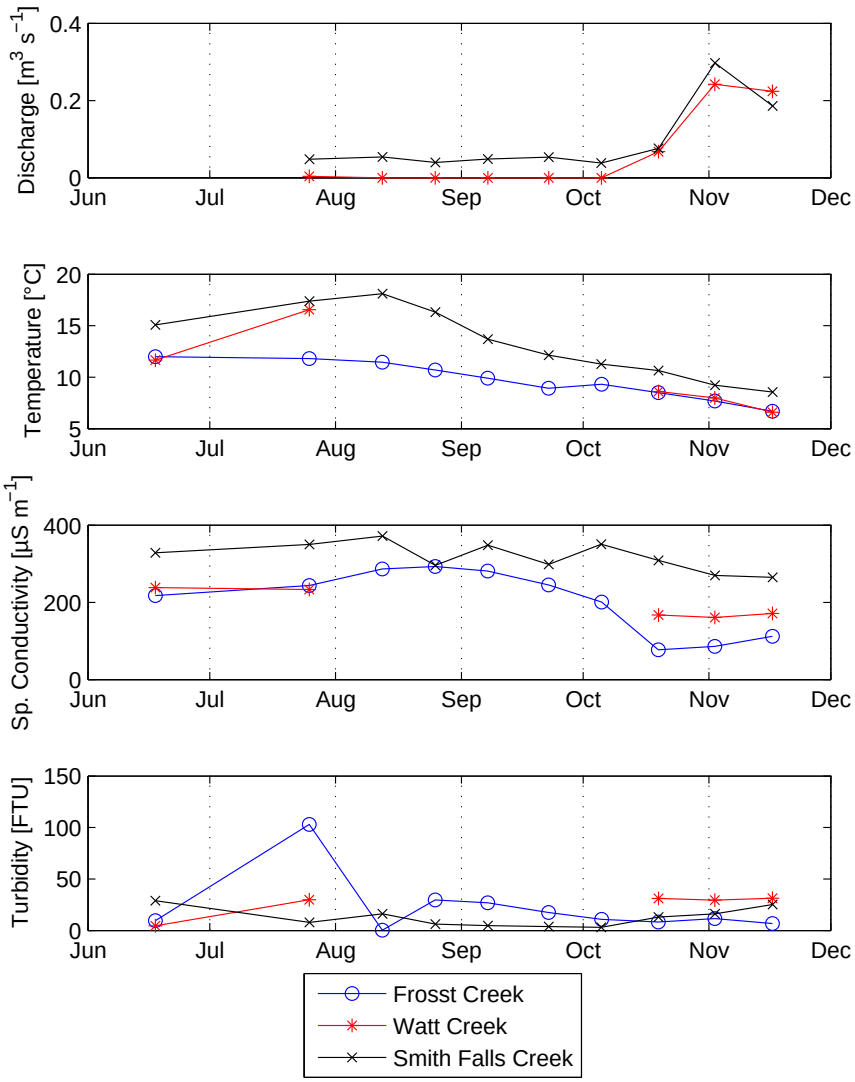

Figure 3.5: Discharge for Watt Creek and Smith Falls Creek, and specific conductivity and turbidity for Frosst Creek, Watt Creek, and Smith Falls Creek. Watt Creek was dry between 12 August 2016 and 5 October 2106.

3.5 Modelling Cultus Lake

Several modelling periods were run in GLM to simulate the thermal characteristics of Cultus Lake. First, the model was calibrated using field data obtained in 2016. A sensitivity analysis was also done for the 2016 calibrated model. Secondly, a hindcast was done for 2009–2016 to validate the calibrated model. Thirdly, another two hindcasts were performed for 2001–2003 to evaluate the regional climate model data by comparing them to observed data. Finally, GLM was run for 2009–2100 for two climate change scenarios.

3.5.1 Calibration Period

Water temperature data collected in 2016 were used to calibrate GLM. The initial profile was set as the spatially averaged temperature profiles binned into 1 m layers as calculated from CTD casts on 28 April. The initial lake depth was set to 42.5 m as provided by the Cultus Lake Park Board. An hourly timestep was used in the model. A summary of the calibration parameters used in the model are shown in Table 3.1. Minimum and maximum layer thicknesses of 0.3 m and 0.9 m, respectively, to ensure that the minimum layer was not so small as to form ice in the winter and that three small layers could mix together to form a larger layer. The extinction coefficient of 0.22 m^{-1} was calculated from the average Secchi depth and PAR profiles over the study period. All aerodynamic and mixing coefficients were set to the default values. Good results were found using albedo mode 3 and cloud mode 4 (see Hipsey, Bruce, et al. 2013 from Yajima and Yamamoto 2015). Wind data were reduced by 5 %, due to higher wind values observed at Abbotsford Airport than at Cultus Lake, likely the result of topographic and predominant atmospheric flow differences. Shortwave radiation was increased by 30 %. This is an increase of the PAR portion of solar radiation from 47 % to 63 %. The conversion between solar radiation and PAR is not direct nor constant. Water vapour, clouds, and the annual solar cycle can cause an increase in the PAR portion of solar radiation. Past observations in College Station, Texas (30.583°'N 96.350°W) resulted in a PAR fraction ranging between 47 % and 58 % of the solar radiation (Britton and Dodd 1976). It is therefore not unreasonable to see a slight increase at higher latitudes where the photoperiod is shorter. Further, the calibrated PAR fraction value of 63 % is within the ±5 % accuracy of the LI-COR PAR sensor. Other meteorological factors did not require adjustment.

Table 3.1: Calibration parameters for GLM setup on Cultus Lake.

Parameter	Default (Hipsey, Bruce, et al. 2014)	Cultus Lake Value (Comments)
Maximum number of layers	N/A	500
Minimum layer volume [m^3]	0.025	0.025
Minimum layer thickness [m]	0.5	0.3
Maximum layer thickness [m]	1.0	0.9 (At least twice the minimum layer thickness)
Extinction coefficient [m^{-1}]	0.2	0.22 (From average Secchi depth)
Bulk aerodynamic coefficient for sensible heat transfer	0.0013	0.0013
Bulk aerodynamic coefficient for latent heat transfer	0.0013	0.0013
Bulk aerodynamic coefficient for transfer of momentum	0.0013	0.0013
Mixing efficiency - convective overturn	0.2	0.2
Mixing efficiency - wind stirring	0.23	0.23
Mixing efficiency - shear production	0.3	0.3
Mixing efficiency - unsteady turbulence (acceleration)	0.51	0.51
Mixing efficiency - Kelvin-Hemlholtz turbulent billows	0.3	0.3
Mixing efficiency of hypolimnetic turbulence	0.5	0.5
Albedo mode	N/A	3
Cloud mode	N/A	4
Wind factor	1.0	0.95 (Correction for values from Abbotsford Airport)
Shortwave factor	1.0	1.3 (Correction for shortwave radiation calculated from PAR)

Table 3.1 – continued from previous page

Parameter	Default	Cultus Lake Value (Comments)
Longwave factor	1.0	1.0
Air temperature factor	1.0	1.0
Relative humidity factor	1.0	1.0
Rain factor	1.0	1.0

The inflow parameters used for GLM are shown in Table 3.2. The stream half-angle set to 60° for all streams. The slope for Frosst Creek is 4 %, or 2.29° (Zubel 2000) and the same slope was assumed for Watt Creek. The slope for Smith Falls Creek was estimated to be higher (4.5 %, 2.58°) because the creek discharges through a culvert beneath the Columbia Valley highway and onto the exposed banks of the lake. The streambed drag coefficient was set to 0.016 (Fisher et al. 1979) for all three streams. Outflow data were not incorporated into the model because the Cultus Lake Park Board attempts to maintain a stable water level throughout the summer by means of stop logs. Therefore, overflow discharges from GLM were used as surrogates for the outflow.

Table 3.2: Inflow parameters for GLM

Inflow	Stream Half Angle (degrees)	Streambed Slope (degrees)	Streambed Drag Coefficient
Frosst Creek	60	1.54	0.016
Watt Creek	60	1.54	0.016
Smith Falls Creek	60	2.58	0.016

3.5.2 Model Evaluation

Observed average lake temperatures and simulated result profiles are shown in Figure 3.6 for each field day. The model replicates the hypolimnetic temperatures very well; however, the model struggles in the spring to replicate the epilimnion. On 20 May, the simulated epilimnion is deeper and the thermocline sharper than observations. Interestingly, the secondary thermocline observed in June was replicated in the model. There is some delay

in the warming of the epilimnion throughout July and August; the observed epilimnetic temperature is up to 1.6 °C warmer than the model on July 25. However, the model performs well in the late summer as the epilimnion begins to cool. The bottom of the metalimnion in the model is not as sharp as what was observed in October and November, this is likely due to an increase in inflow discharge in the fall which is eroding the simulated thermocline. Finally, on December 8, the observed and simulated results are very similar as the lake begins to completely mix.

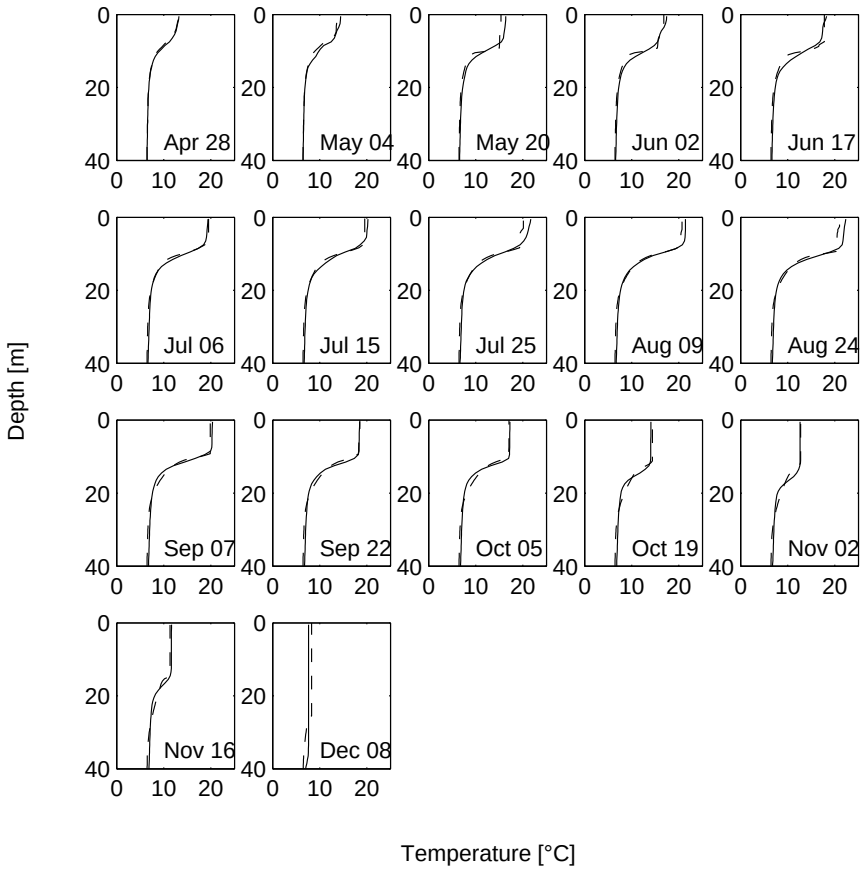

Figure 3.6: Model evaluation for the 2016 calibration period. Solid lines indicated the spatially average temperature profile. Dashed lines are the simulated results.

Root-mean-square error (RMSE) between the average observed and simulated temperatures was calculated to provide a single number for the error in the profile for each field day. RMSE is given by:

$$RMSE = \sqrt{\frac{\sum_{i=1}^{n}(\overline{x}_i - x_i)^2}{n}} \tag{3.2}$$

where $\overline{x}_i$ and x_i are the simulated and observed values at each point i, respectively. This equation can also be normalized to give the normalized root mean square error (NRMSE):

$$NMRSE = \frac{RMSE}{x_{max} - x_{min}} \tag{3.3}$$

where x_{max} and x_{min} are the maximum and minimized observed values for each day. A time-series of the RMSE for the 2016 calibration period is presented in Figure 3.7. The maximum observed spatial temperature variation for the lake is shown alongside the RMSE. This variation was calculated by determining the maximum difference between casts for each 1 m layer and taking the maximum of these values from each field day; it represents a metric for the acceptable level of error for the model. The RMSE averages 0.46 °C throughout the simulation and is lower than the maximum observed spatial temperature variation in the lake for each profile, which has an average of 1.64 °C. For the final field day on 8 December 2016, the RMSE is larger than the temperature variation. Only a single profile was completed to the bottom of the lake due to difficult weather conditions, therefore a complete survey of the lake was unattainable.

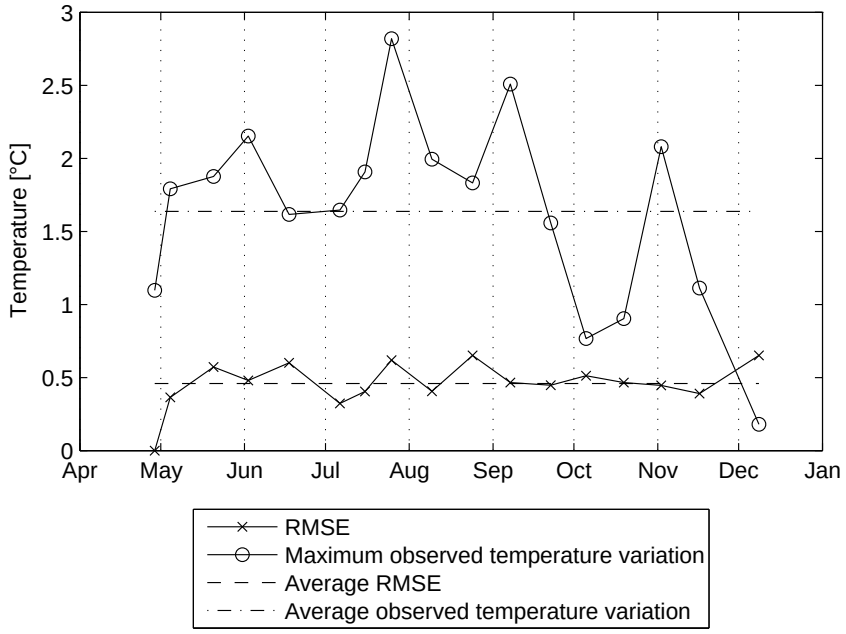

Figure 3.7: RMSE for each 2016 temperature profile compared to the maximum observed temperature variation for each field day.

Further model evaluation was done by comparing the observed and simulated heat content. Total lake heat content was determined by summing the heat content of the 1 m layers:

$$H = \frac{1}{A_0} \sum_{z_0}^{z_m} c_p(T - T_{TMD})\rho A \Delta z \tag{3.4}$$

where A_0 is the lake surface area, z_m is the maximum depth, c_p is the heat capacity of water, T is the temperature, T_{TMD} is the temperature of maximum density, ρ is the density, and A is the area of each layer. The MATLAB TEOS-10 toolbox was used to calculate the values for c_p, T_{TMD}, and ρ assuming the chemical composition of seawater. The heat content indicates the amount of heat released upon cooling to the temperature of maximum density (Wetzel 2001) (roughly 4 °C, depending on salinity and depth). A negative value of H indicates the amount of heat required to raise the temperature of the lake to the temperature of maximum density (Wetzel

2001). The modelled heat content roughly follows the same increasing trend as the observed data throughout the spring (Figure 3.8). A minor increase in heat content was simulated in early June that was not captured in the CTD casts, but is seen in the mooring data. The observed peak heat content in late August was not simulated in the model. The results correlate well throughout September, but the simulated heat content is lower throughout the fall but does not reach the minimum observed on 8 December.

Heat content was also calculated assuming pure water (i.e. no salinity) to determine the effects of salinity and potential error. The heat content RMSE over the calibration period was 2.4 MJ m^{-2}, or a NRMSE of 0.4 %. The effects of salinity are therefore negligible and are ignored in the model hindcasts (Sections 3.5.4 and 3.5.5) and forecasts (Section 3.6); however, future studies incorporating nutrient loading scenarios should include salinity in their calculations.

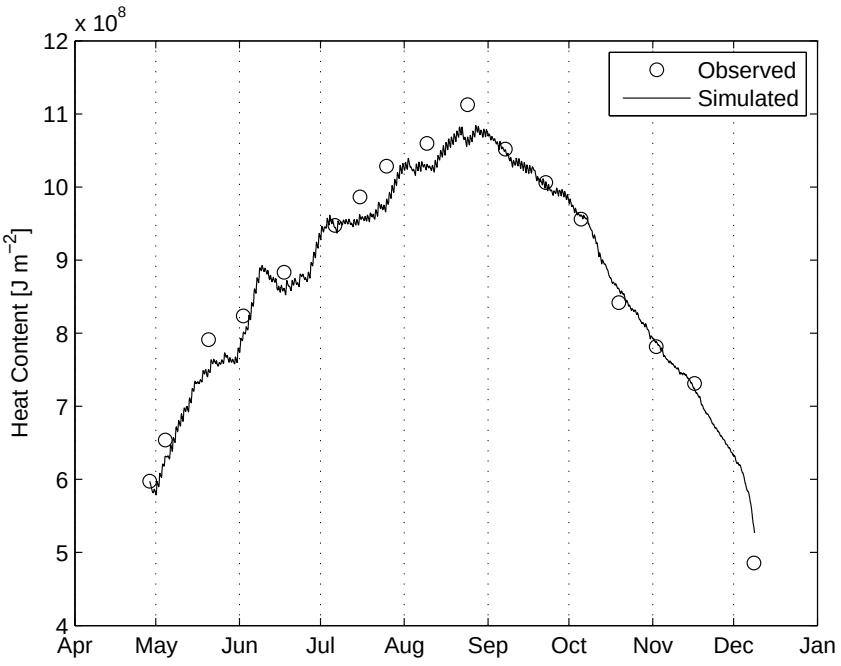

Figure 3.8: Observed and simulated total heat content of Cultus Lake for 2016.

3.5.3 Sensitivity Analysis

The finalized model was subject to an elementary effects sensitivity analysis on the most uncertain parameters and those parameters that would likely be affected by climate change: extinction coefficient, meteorological multiplication factors, inflow half-angle, and inflow slope. A simple Morris screening method was used to evaluate the effects of the inputs on the model. The model inputs were evaluated between ± 50 % of their calibrated 2016 values (Tables 3.1 and 3.2) and compared to their effects on the total NRMSE for water temperature. The Morris method is described in detail in Campolongo et al. (2007) but gives the elementary effects as:

$$EE_i(\mathbf{X}) = \frac{Y(X_1, \ldots, X_{i-1}, X_i + \Delta, X_{i+1}, \ldots, X_k) - Y(\mathbf{X})}{\Delta} \tag{3.5}$$

where $\mathbf{X} = (X_1, X_2, \ldots, X_k)$ is any value within ± 50 %, and $\Delta = p/[2(p-1)]$ with p equal to the number of repetitions computed per elementary factor, here $p = 20$ was chosen to ensure enough calculations were performed. A criterion to rank the effects of the inputs is defined as the mean of the absolute values of the elementary effects, μ_i^*. The values for μ_i^* are shown in Table 3.3. The model is highly sensitive to changes in the longwave, shortwave, and air temperature factors. These parameters account for the bulk of the heat flux in the model, so it is expected that they would contribute to model sensitivity. The model is moderately sensitive to wind speeds, and has little sensitivity to the extinction coefficient and relative humidity. There is very little sensitivity to the rain factor and inflow slopes and half angles.

Table 3.3: Sensitivity analysis results, and normalized root-mean-square error of the observed and CanRCM4 historical data for 2001–2003. GLM input parameters are ranked by the mean of their elemental effects (μ_i^*).

Parameter, i	μ_i^*	NRMSE of Input Data
Longwave factor	0.703	0.179[1]
Shortwave factor	0.430	0.271
Air temperature factor	0.404	0.121
Wind factor	0.122	0.193[2]
Extinction coefficient	0.085	N/A
Relative humidity factor	0.063	0.269[2]
Frosst Creek half angle	0.013	N/A
Frosst Creek slope	0.006	N/A
Rain factor	0.004	0.160[2]
Smith Falls Creek slope	0.004	N/A
Watt Creek half angle	0.004	N/A
Smith Falls Creek half angle	0.004	N/A
Watt Creek slope	0.003	N/A

[1] Calculated longwave radiation from observed cloud cover data at Abbotsford Airport following Yajima and Yamamoto (2015).
[2] Calculated after bias correction for CanRCM4 data.

3.5.4 Hindcast (2009–2016)

The calibrated model was hindcast to validate the model using monthly DFO data obtained near station CL2 at monthly intervals beginning 17 February 2009. Hourly air temperature and relative humidity from Abbotsford Airport were used for the period between 17 February 2009 until 5 June 2011 when the Cultus Lake weather station was installed. Daily precipitation was obtained from the Chilliwack weather station until it was decommissioned on 31 August 2012, subsequently the Abbotsford precipitation data were used. Inflow data for 2011–2013 were obtained from Putt (2014). Because the inflow data are not consistent, the water level drops between 2009 and 2011 until the data from Putt (2014) are used, and again between 2013 and 2016. However, the water level drop is minimal and less than 2 m. Validation techniques were the same as those for the 2016 calibration. The average temperature RMSE over this period is 1.10 °C (Figure 3.9). A yearly cycle is seen in the RMSE, with peaks in the summer and minima in the winter. The RMSE shows large spikes, near or above 2 °C in the summers of

2009–2011 and 2014. Overall, the average RMSE is less than the observed temperature variation limit for 2016. The total lake heat content was also used to evaluate the model (Figure 3.10). The trends roughly follow that of the observed heat content, but some peaks do occur in the summers of 2009, 2010, 2011, and 2014. These are the same years where the RMSE was also at a maximum.

There are clearly some heating biases in the model. Possible errors may be from the air temperature data being obtained from Abbotsford Airport prior to the commissioning of the Cultus Lake weather station in the summer of 2012. Additionally, observed temperature profiles were only obtained at one location prior to 2016 near the upstream end of the lake, so there would be some error expected from internal seiching, as determined from the spatial variability in 2016. Furthermore, inflow data were provided for only 2011–2013 and again in 2016 which may account for some error. While the model is not able to perfectly resolve the temperature in the lake—partially due to disparities in meteorological measurements—it does a good job at reproducing seasonal trends. This reinforces the statement in Hipsey, Bruce, et al. (2014) that the model is best intended for use in long-term investigations.

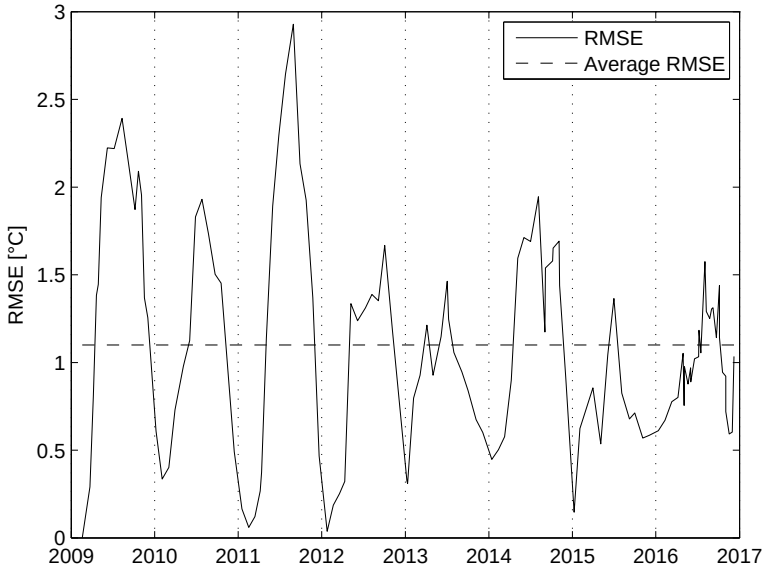

Figure 3.9: RMSE for each field day of the hindcast model (2009–2016).

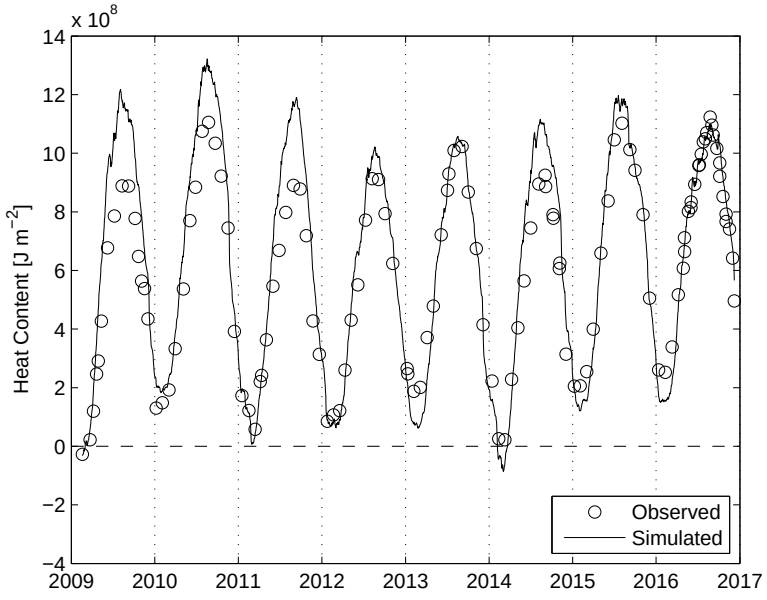

Figure 3.10: Daily observed and simulated heat content (2009–2016).

3.5.5 Forecast Data Evaluation (2001–2003)

Corrected CanRCM4 meteorological data from the historical run were compared to observations taken at Abbotsford Airport in 2001–2003. The NRMSE was calculated between the observed and synthetic data and compared to the sensitivity analysis results (Table 3.3). While the NRMSE of all parameters was within 30 %, it was found that the seasonality of the synthetic relative humidity did not match that of the observed data: the observed relative humidity was much lower in the summer than that of the synthetic data. A bias correction was performed to adjust the seasonality differences following the quantile mapping (Panofsky and Brier 1958) of the cumulative frequency distributions for the parameters. For any climate variable, this can be written as:

$$x_{m\text{-}corr}(t) = F^{-1}_{o\text{-}ref}(F_{m\text{-}ref}(x_{m\text{-}raw}(t)) \tag{3.6}$$

where $x_{m\text{-}corr}$ is the corrected modelled value at each timestep, $x_{m\text{-}raw}$ is the raw modelled value at each timestep, and F is the distribution function for the observed (o) and modelled (m) data over the reference period (a Weibull distribution was used in this case). A time period of 1953–2005 was used for the reference data. The bias correction was calculated for each month to ensure the seasonal cycle was properly corrected. Precipitation and wind speeds were also corrected in this manner. The correction of precipitation eliminated the so-called *drizzle effect* (Gutowski Jr et al. 2003) found in climate models where the models produce too many low intensity rain events compared to observations. Other meteorological parameters were not bias corrected due to their low NRMSE and relatively similar seasonality and distribution curves to the observed data. This seasonal similarity can be attributed to the small grid spacing of the CanRCM4 model that is able to refine micro-climates better than global models. The model nevertheless remains highly sensitive to longwave radiation. In this study, observed cloud fraction was used to calculate longwave radiation, while incoming longwave radiation was obtained for the CanRCM4 model runs. Cloud feedbacks are the largest source of uncertainty in climate models and remain difficult to quantify (von Salzen et al. 2013). The model is also sensitive to shortwave radiation which also has a high NRMSE. However, this can be attributed to the cloud fraction uncertainty. Air temperature, for which the model has high sensitivity, had the lowest NRMSE for the synthetic data. Wind speeds had a high NRMSE, but the model is less sensitive to this parameter. For the bias corrected relative humidity, the NRMSE is still high but the model has low sensitivity. The model is largely insensitive to rain which also has a

low NRMSE.

Highly porous soil in the vicinity of Cultus Lake results in much of the precipitation (roughly 63 %) draining into groundwater (Zubel 2000), while approximately a third of the rainfall becomes surface runoff (Scibek and Allen 2006). Total runoff data from CanRCM4, which includes drainage to groundwater, were therefore halved to determine surface runoff, then subsequently multiplied by each stream's drainage area to determine daily inflows. A baseflow of 0.2 $m^3 s^{-1}$ was added to the inflow for Frosst Creek, while a baseflow of 0.03 $m^3 s^{-1}$ was added to the inflow for Smith Falls Creek, as determined from 2016 flow data, to account for groundwater running into each creek. No baseflow was added to the intermittent Watt Creek. Forecast stream temperatures were determined using the correlation between air temperatures and stream temperatures for the 2016 season.

A verification of the CanRCM4 output adjustments was done by running two simulations for 2001–2003: one using the CanRCM4 historical simulation and the other using observed data at Abbotsford Airport. Observed and bias corrected synthetic wind speeds at Abbotsford Airport were again reduced by 5 %, but a shortwave radiation correction was not required. Again, the water temperature RMSE and heat content were used to evaluate the model. The RMSE follows a similar trend to the 2009–2016 hindcast (Figure 3.11). The RMSE increases in the summer and returns to a minimum in the winter. Unfortunately, observed inflow data were not available for this period, but from Table 3.3 the model has a low sensitivity to inflows. The average RMSE over the simulation period was similar for both scenarios: 0.90 °C and 0.81 °C for the observed and synthetic scenarios, respectively. These results are comparable to those of the 2009–2016 hindcast and less than the observed maximum temperature variation in the lake for 2016. Heat content was also evaluated for both scenarios and compared to the observed data (Figure 3.12). The scenario using observed data at Abbotsford Airport typically has a higher heat content throughout the simulation period than the observed data. This result is similar to the 2009–2016 hindcast years where temperature data were obtained from Abbotsford, reinforcing that the model is sensitive to air temperature. The simulation using synthetic CanRCM4 historical data has a heat content that roughly follows what was observed. However, the heat content increases at a reduced rate in the spring, but follows a similar decline in the fall to what was observed. The heat content also reaches a minimum earlier in the year than what was measured.

Overall, the bias corrected CanRCM4 data provide similar simulation results to those obtained using the observed meteorological data. The high-

est errors are observed in the summer; however, they are generally less than the spatial variation in the lake as determined from the 2016 data. The bias correction technique described here can therefore be applied to the forecast CanRCM4 meteorological data to be confidently used to forecast future lake conditions.

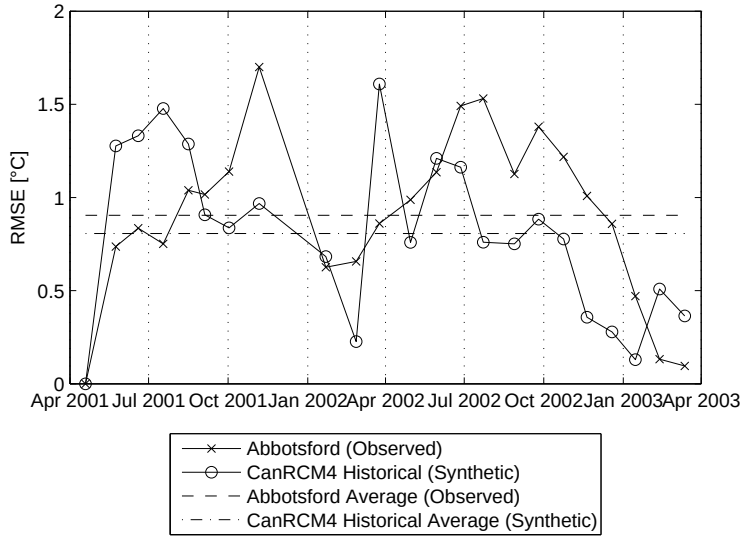

Figure 3.11: RMSE for each field day of the hindcast model using observed and synthetic meteorological data (2001–2003).

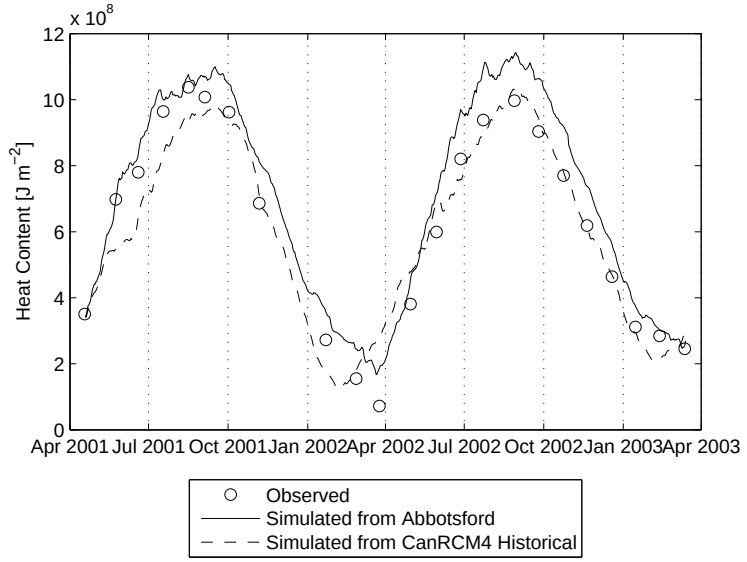

Figure 3.12: Daily observed and simulated heat content using observed and synthetic meteorological data (2001–2003).

3.6 Historical and Forecast Results (1923–2100)

Two forecast scenarios were run in GLM for 2009–2100. The eight year overlap between the forecast scenarios and the observed data provides a good evaluation for the early years of the CanRCM4 forecast scenarios. The results from the forecast years were compared to historical data dating to the 1920s.

3.6.1 Heat Content

Daily heat content was calculated for the historical data. To calculate the heat content, the historical data obtained from Foerster (1925) and Ricker (1937) for the periods of 1923, 1927–1929, and 1932–1936; and from DFO for 2001–2003 and 2009–2016 were linearly interpolated to obtain daily values. This was combined with the semimonthly data obtained in 2016. A linear trend was fit to the data which indicates the yearly average heat content (Figure 3.13. This trend increases at a rate of + 0.80 $MJ\,m^{-2}$ per year over the observed period. The trend may not in reality be linear; however, it should be noted that increased heating compared to the 1930s was observed in the 1960s–1970s (Goodlad et al. 1974). Additionally, measurements from 1923 results in an anomalously high heat content, peaking at 1.47 $GJ\,m^{-2}$. Hypolimnetic temperatures were recorded at or above 9 °C in 1923, which is significantly warmer than those observed in 2016. Summer air temperatures were not unusually warm for this year (Foerster 1925) that would cause elevated hypolimnetic temperatures, so it is possible that the temperature of the water volume in the modified deep-sea thermometer warmed when the thermometer was hauled to the surface. Winter heat content minima are historically continually approaching zero. This shows that the lake was becoming isothermal and approaching the temperature of maximum density. For years where the heat content was negative, the lake temperatures had cooled below the temperature of maximum density and the lake was potentially inversely stratified.

Future climate scenarios indicate a continued increase in total lake heat content (Figure 3.13). The RCP4.5 scenario indicates a heating rate more than double the historical trend (+ 2.0 $MJ\,m^{-2}$ per year compared to + 0.80 $MJ\,m^{-2}$, respectively). The RCP8.5 scenario shows a sharp increase in heating rate to + 4.2 $MJ\,m^{-2}$ per year, over twice that of the RCP4.5 scenario. In both scenarios, the winter heat content minima are predicted to continually increase above zero, with some anomalous years at or below zero. For the RCP8.5 scenario, the years where the heat content is below

zero occur near the beginning of the simulation, whereas RCP4.5 has two years (2042–2043, 2044–2045) where the heat content minimum is below zero. This trend means that lake temperatures are on average remaining above the temperature of maximum density throughout the year. Therefore, there would be no possibility of inverse stratification.

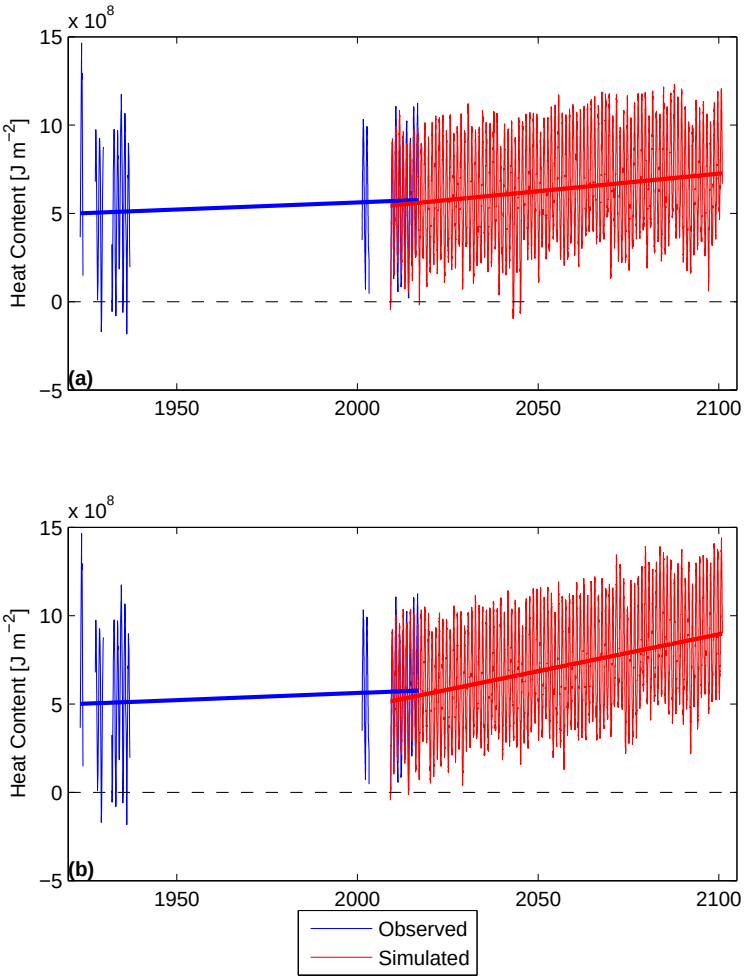

Figure 3.13: Historical observed heat content and projected heat content of Cultus Lake for RCP4.5 (a) and RCP8.5 (b). Linear trend lines are shown in bold.

3.6.2 Stability and Stratification

Lake stability is the amount of work required to completely mix the lake to a uniform temperature (Wetzel 2001). It is therefore a good indicator of the strength of stratification. The stability increases throughout summer as the epilimnion warms and stratification intensifies; when the lake is completely mixed, the stability returns to zero. Unlike heat content, stability is not referenced to a specific temperature, therefore a stability of zero could indicate mixing above or below the temperature of maximum density. The lake stability was calculated using the Schmidt Stability Index (SSI) as formulated by Idso (1973):

$$SSI = \frac{g}{A_0} \sum_{z_0}^{z_m} (z - z_{\overline{\rho}})(\rho - \overline{\rho}) A \Delta z \tag{3.7}$$

where g is the gravitational constant, $\overline{\rho}$ is the average density, and $z_{\overline{\rho}}$ is the depth of average density calculated from:

$$\overline{\rho} = \frac{\sum_{z_0}^{z_m} \rho z A \Delta z}{\sum_{z_0}^{z_m} \rho A \Delta z} \tag{3.8}$$

$$z_{\overline{\rho}} = \frac{\sum_{z_0}^{z_m} \rho A \Delta z}{\sum_{z_0}^{z_m} A \Delta z} \tag{3.9}$$

The historical SSI was calculated for all observed historical data and interpolated to obtain daily values. A linear trend was fit to the historical and projected data which indicates the yearly average SSI (Figure 3.14). Historically, the SSI increased at a rate of + 2.19 J m^{-2} per year with summer peaks between 2000 J m^{-2} and 3000 J m^{-2}. For the climate change scenarios, the SSI is expected to increase at a rate of + 2.6 J m^{-2} per year and + 6.5 J m^{-2} per year for climate change scenarios RCP4.5 and RCP8.5, respectively. For RCP4.5, the SSI begins to approaches but does not consistently seasonally peak above 3000 J m^{-2} by 2100; whereas the seasonal peaks shift to above 3000 J m^{-2} by 2100 for RCP8.5 and begin to approach 4000 J m^{-2}. This is a significant increase to what was observed historically and further isolates the hypolimnion from the epilimnion due to an increase in stratification strength.

Stratification season was determined using three methods: (i) periods when the difference between the surface and bottom temperatures was greater

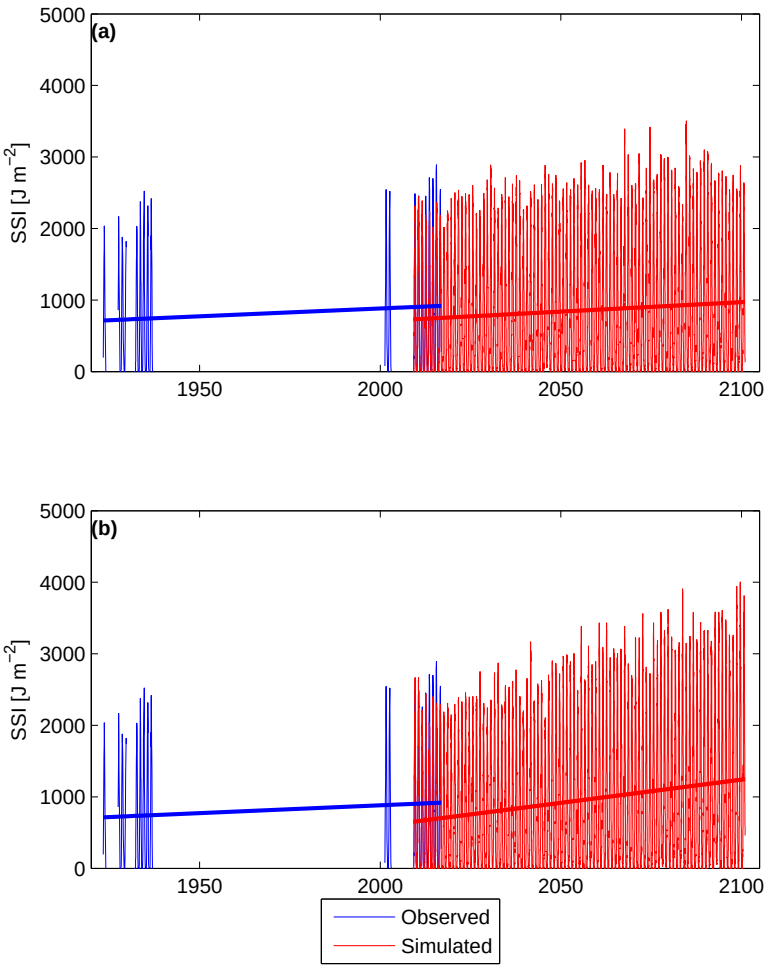

Figure 3.14: Historical observed Schmidt Stability Index and Schmidt Stability Index of Cultus Lake for RCP4.5 (a) and RCP8.5 (b). Linear trend lines are shown in bold.

than 1 °C, (ii) the SSI was greater than 30 J m^{-2} (Engelhardt and Kirillin 2014), and (iii) a thermocline was established based on the traditional definition of a vertical temperature change greater than 1 °C m^{-1} (Ricker 1937; Wetzel 2001). The surface temperature was also required to be at or greater

than 4 °C to remove periods where the lake may be inversely stratified. After preliminary calculations, it was noticed that the lake was remaining stratified beyond 31 December after some years of warming had elapsed. A *lake new year* was therefore established as February 20 and defined as the date where Cultus Lake was typically completely unstratified following the above definitions of stratification. By shifting the new year, calculations could then be done by finding the first and last dates of the year where the threshold values were crossed. All three methods saw an increase in duration of stratification for both warming scenarios (Figure 3.15). A linear trend was fit to the data and is summarized in Table 3.4. Overall, the thermocline method gives a more conservative result but requires a vertical grid spacing of 1 m, which is not available in the historical data. The SSI threshold method was henceforth chosen as the representative method to calculate historical and future length of stratification season, but the top to bottom temperature difference method could equally have been chosen because the two methods produce similar results.

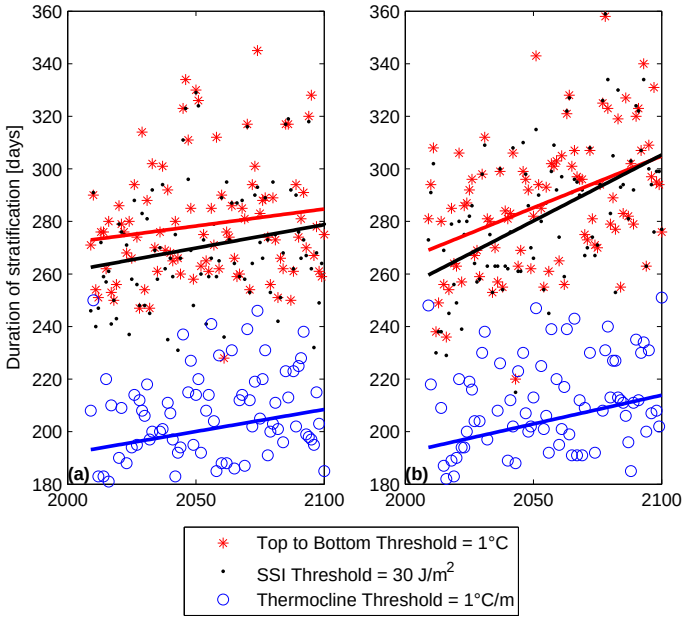

Figure 3.15: Comparison of the three methods used to evaluate thermal stratification season for future climate scenarios RCP4.5 (a) and RCP8.5 (b). Linear trend lines are shown in bold.

Table 3.4: Comparison of the duration of stratification for the three methods. Days shown are for the linear trend lines from Figure 3.15.

		(i) Temperature difference surface–bottom	(ii) SSI	(iii) Thermocline
RCP 4.5	Days stratified in 2009	273	263	193
	Days stratified in 2100	285	279	209
	Rate of change [days/year]	0.13	0.18	0.17
RCP 8.5	Days stratified in 2009	269	260	194
	Days stratified in 2100	305	305	214
	Rate of change [days/year]	0.39	0.50	0.22

A comparison of the forecast results to the historical duration of stratification was done to evaluate the effects of climate change. Historical temperature data were linearly interpolated between cast dates to obtain a daily SSI in order to calculate when stratification occurs and breaks down. A linear trend was calculated for the total duration of stratification. This trend excluded the total duration calculated from 1923, 1924, and 1927–1929 because complete monthly data sets are not available which resulted in large interpolation steps. The linear trend increases from 249 days to 266 days, or a rate of 0.18 days per year (Figure 3.16). With the SSI threshold method, The rate of increase in duration of stratification is expected to stay the same with climate change at 0.18 days per year for RCP4.5 and but expected to more than double to 0.50 days per year for RCP8.5.

Further investigation was done determine the onset and breakup of thermal stratification (Figure 3.17). Historically, the onset of stratification occurred around 10 April in the 1920s–1930s, and has shifted 18 days earlier to 23 March in the 2010s. For RCP4.5, the onset of stratification remains relatively steady and occurs around 5 April, while for RCP8.5, the onset of

stratification increases slightly from 4 April to 27 March. There are therefore no substantial changes to the onset of stratification predicted for future warming scenarios out to 2100 AD. Stratification breakup has historically been relatively steady and occurred around 15 December. However, major changes in stratification breakup are seen in the climate forecast: a shift to 12 January is predicted for RCP4.5 and a shift to 25 January for RCP8.5. Furthermore, breakup of stratification did not occur in some forecast years. These years were the winters of 2045–2046 and 2050–2051 for RCP4.5, and 2063–2064, 2077–2078, 2090–2091, and 2092–2093 for RCP8.5. For these winters, complete lake mixing did not occur but this does not necessarily mean the lake was stratified for 365 days as in Figure 3.15. If the onset of stratification of the preceding year occurred after 20 February (lake new year), the duration of stratification would therefore be the difference between the date of onset of stratification and 20 February of the following year. The total duration of stratification would then be the sum of the duration of stratification of the two years affected (e.g. 2045 and 2046), which could be, but is not necessarily, greater than 365 days.

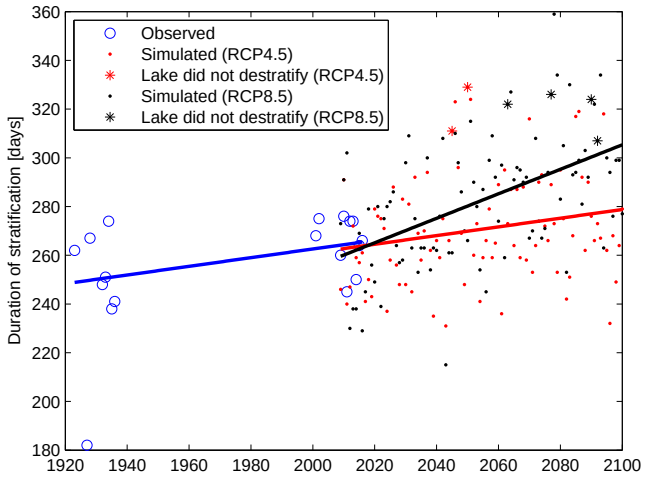

Figure 3.16: Historical and predicted duration of thermal stratification for RCP4.5 and RCP8.5. Linear trend lines are shown in bold.

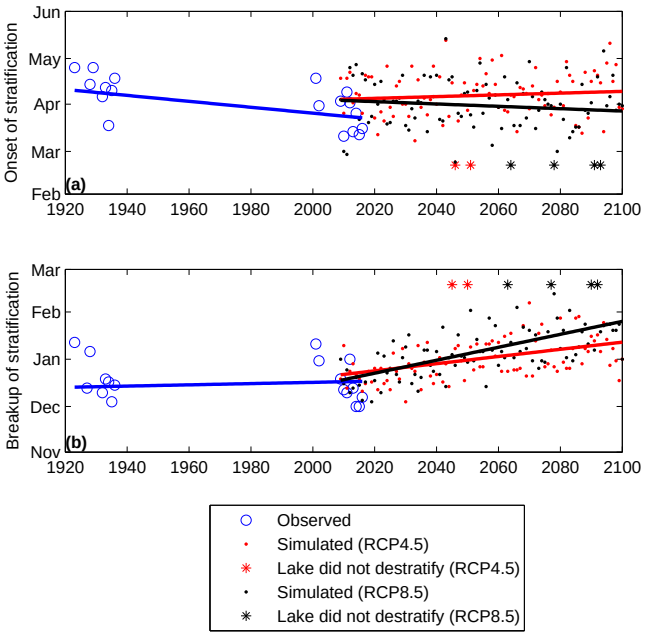

Figure 3.17: Historical and predicted onset (a) and breakup (b) of thermal stratification. Linear trend lines are shown in bold.

A small disparity in the onset of stratification is seen in trendlines of the 2009–2016 overlap for the observed and simulated data. It is important to note that the observed data were linearly interpolated between monthly measurements so an error on the order of several days to weeks is expected. Interestingly, the simulated onset of stratification is similar to the date of onset in the early 20^{th} century. The error in the linear interpolation of the measurements by Ricker (1937) is expected to be on the order of days because of the semi-monthly observation interval. There is very little change in the projected onset of stratification in both climate scenarios, indicating that the onset of stratification is not expected to significantly shift with climate change. The bulk of the increase in the duration of stratification therefore comes from a delayed breakup of stratification. Stormy events with high winds are frequent in the late fall and early winter on the west coast. The lake is remaining stable for a longer period from the increase and retention of heat and preventing wind mixing rather than becoming stable at an earlier period. Winds in the late winter are keeping the lake well mixed and preventing the lake from becoming thermally stratified.

Inverse stratification was also investigated using SSI threshold method. This was constrained by requiring the surface temperature to be below 4 °C. Using this method, inverse stratification was neither detected for the historical data nor the forecast results. Therefore, the potential effects of inverse stratification are not a concern and Cultus Lake can be classified as warm monomictic.

3.6.3 Surface and Outflow Temperatures

River temperatures in Sweltzer River were analyzed for potential fish mortality impacts on Sockeye Salmon. Surface temperatures from Cultus Lake were used as surrogates for river temperature because they have been previously shown to have similar values (Shortreed 2007). In recent years, Sockeye Salmon mortality has increased due to an earlier migration time into water courses with warm temperatures (Cooke et al. 2004). Sockeye Salmon have been shown to have increased mortality in migration temperatures greater than 18 °C (Brett 1971; Crossin et al. 2008). The Cultus Lake population typically runs between early August and early December (Shortreed 2007), so mean monthly river temperatures have been calculated for the months of August–November (Figure 3.18). Historically, the Sweltzer River temperature has been above the 18 °C threshold in August and September and has been increasing at a rate of 0.016 °C and 0.013 °C per year for August and September, respectively since 1923. October river temperatures have

been increasing at a rate of 0.010 °C per year, while river temperatures in November have not seen a significant historical increase. River temperatures are projected to increase at a much higher rate in both warming scenarios. For RCP4.5, the river temperatures are projected to increase at a rate of 0.031 °C per year, 0.025 °C per year, 0.018 °C per year, and 0.016 °C per year for August, September, October, and November, respectively. Heating rates for RCP8.5 are 0.069 °C per year, 0.069 °C per year, 0.059 °C per year, and 0.046 °C per year for August, September, October, and November, respectively. The October river temperatures in RCP4.5 approach and are occasionally greater than 18 °C by 2100, whereas the RCP8.5 October river temperatures cross the 18 °C threshold in 2072 and reach 20 °C by 2100. For both warming scenarios, the November river temperatures remain below the mortality threshold. The predominant salmon migration into Cultus Lake typically occurs in late September and early October (Cultus Sockeye Recovery Team 2005), so temperature increases beyond the 18 °C threshold during this period, such as what is projected for RCP8.5, would have dire impacts on the Cultus Lake Sockeye Salmon population.

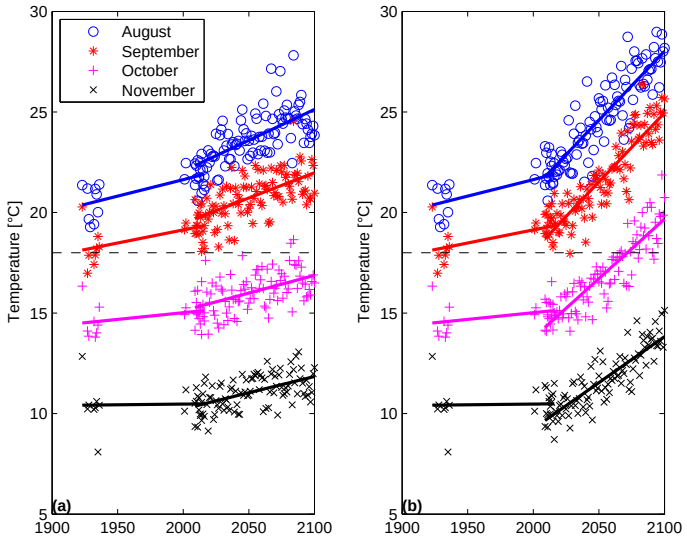

Figure 3.18: Historical and predicted surface and outflow temperatures for RCP4.5 (a) and RCP8.5 (b). Linear trend lines are shown in bold. Dashed line at 18 °C indicates temperature threshold for Sockeye Salmon.

Chapter 4

Discussion

Climate change has the capacity to significantly affect the physical processes within lakes by modifying heat exchanges between the atmosphere and the water surface. Lakes act as sentinels of climate change because they elicit strong responses in their thermal and ecosystem structures (Adrian et al. 2009). The analysis of the thermal characteristics of Cultus Lake presented here provides a good understanding of the historical response of Cultus Lake to climate change since the 1920s. Two potential climate change scenarios (RCP4.5 and RCP8.5) indicate that the thermal characteristics of the lake are projected to change significantly through 2100 AD. The lake ecosystem is expected to respond to these changes, likely further exacerbating threats to extinction for Sockeye Salmon and Cultus Lake Pygmy Sculpin.

4.1 Potential Changes to the Lake Mixing Regime

Epilimnetic and surface water temperatures often exhibit a strong response to warming air temperatures (Adrian et al. 2009). Air temperatures in the Fraser Valley are projected to increase by + 2.8 °C through the 21st century (Pacific Climate Impacts Consortium 2012). Resultant heating of the water column from climate change can increase the total lake heat content and lake stability thereby increasing the duration of thermal stratification (Weinberger and Vetter 2014; Sahoo et al. 2015).

The current mixing period of Cultus Lake typically begins in December when the lake becomes isothermal at temperatures around 7 °C. During circulation, the lake cools to the temperature of maximum density (roughly 4 °C). In some years the lake has been observed by Ricker (1937), DFO, and in the winter of 2016–2017 to cool, isothermally, below 4 °C without inversely stratifying. Under current conditions, wind continuously mixes the lake throughout the winter below the temperature of maximum density. Winter mixing typically lasts until late March to early April at which point the lake becomes thermally stratified. The heat content projections for

the lake indicate that complete mixing will occur at temperatures at or above 4 °C with no possibility of inverse stratification. So, at the onset of stratification, hypolimnetic temperatures would already be above 4 °C leading to an oligomictic state, described as having rare turnover at irregular interannual intervals and temperatures remaining above 4 °C (Wetzel 2001).

Warm monomictic lakes are particularly sensitive to climate changes because their single mixing period in the winter can be shortened with increasing water temperatures in a shift towards an oligomictic state (Livingstone 2008; Adrian et al. 2009). A shift in the mixing regime of Cultus Lake from monomictic to oligomictic is possible in the future under more extreme climate change scenarios (e.g. RCP8.5) as increased heating is expected to continue affecting the timing and duration of thermal stratification. The onset of thermal stratification currently occurs 18 days earlier than historical observations in the 1920s and 1930s, while the breakup of stratification has not seen a significant historical shift, based on a linear interpolation of semi-monthly to monthly thermal profiles. These trends are unique compared to larger lakes in North America, namely Lake Tahoe (Sahoo et al. 2015) and Lake Simcoe (Stainsby et al. 2011) in which the onset of stratification is occurring earlier and the breakup of stratification is occurring later in the year compared to historical values. Nevertheless, the duration of summer stratification in all cases has historically been increasing. Projections for Cultus Lake show that the onset of thermal stratification is expected to remain steady, whereas the breakup of thermal stratification is projected to occur a month later by 2100. Comparatively, a climate change study on Lake Tahoe resulted in an onset of stratification 16 days earlier and a breakup of stratification 22 days later compared to present values by 2100 (Sahoo et al. 2015). Thus, regionality and geomorphology are expected to influence the timing of onset and breakup of thermal stratification with increased heating from climate change. Model projections show Cultus Lake is shifting towards an oligomictic mixing regime, but not yet becoming oligomictic by 2100. Only two years were identified as having no mixing in the RCP4.5 warming scenario, which occurred at seemingly random times (2045–2046 and 2050–2051). By the end of the study period, the length of stratification season was 279 days; a mixing regime shift would therefore not be expected to fully occur for moderate warming scenarios. However, in the RCP8.5 scenario, turnover did not occur in four years towards the end of the simulation (2063–2064, 2077–2078, 2090–2091, and 2092–2093) with the duration of stratification increasing to 305 days by the end of the study period. This suggests that with increased warming beyond 2100, the lake will become oligomictic and possibly shift to meromixis (incomplete water

column mixing) under an extreme climate change scenario.

4.2 Implications of Increased Climate Warming on Ecosystem Structure and Functioning

Freshwater fish are poikilotherms that cannot regulate body temperature, and thus are dependent upon and sensitive to the temperature of their surroundings (Ficke et al. 2007). Cold-water fish species have evolved to survive within specific thermal tolerances, and their physiological processes (e.g. growth, metabolism, and reproduction) and behaviours (e.g. diurnal vertical migration) are directly influenced by changes in surrounding temperature (Pörtner and Farrell 2008; Healey 2011). Cultus Lake hosts two fish species at-risk: the Cultus Lake population of Sockeye Salmon, and the Cultus Pygmy Sculpin (SARA 2002; COSEWIC 2003, 2010); any changes in their environment are predicted to have drastic consequences (SARA 2002; COSEWIC 2003, 2010). The modelling efforts presented here indicate that the total lake heat content has increased since the early 1920s by + 0.80 MJ m^{-2} per year and is projected to markedly increase by + 2.0 MJ m^{-2} per year and + 4.2 MJ m^{-2} per year for RCP4.5 and RCP8.5, respectively, with isothermal temperatures remaining above 4 °C, and potentially deleterious lake ecosystem alterations for species-at-risk.

Increased lake heating can have significant effects on Sockeye Salmon throughout their life cycle (Crozier et al. 2008; Pörtner and Farrell 2008; Healey 2011). In the egg and alevin stage of the Sockeye Salmon life cycle, warmer water temperatures increase metabolic rates, leading to the development of smaller fry, as well as a reduction in disease resistance (Healey 2011). Embryos may also develop faster leading to earlier hatching and emergence, which can present a phenological shift relative to zooplankton prey availability (D. E. Schindler et al. 2005; Healey 2011). Juvenile Sockeye Salmon exhibit a diel vertical migration within the water column, feeding on zooplankton in the epilimnion and metalimnion at night and returning to the bottom of the lake during the day, presumably to evade predators (Clark and Levy 1988; Levy 1990; Scheuerell and D. E. Schindler 2003; Cultus Sockeye Recovery Team 2005). Warmer water temperatures and an increased metabolic demand will require Sockeye Salmon to feed more frequently and may increase their risk of predation (Healey 2011), otherwise an increased metabolic rate would lead to smaller fry sizes and potential reductions in winter survival when food is less abundant (Healey 2011). A reduction in fry size can lead to either smaller smolts which have reduced

survival rates in a marine environment, or fry may delay smolting by a year resulting in fewer smolts migrating to the ocean (Healey 2011).

Recent decades have been marked by a decrease in the number of Sockeye Salmon returning to Cultus Lake (Shortreed 2007). The salmon that are returning are making their run earlier in the season which has had great effects on pre-spawn mortality (Cultus Sockeye Recovery Team 2005; Shortreed 2007). Sockeye Salmon have been shown to have an increased mortality at or above temperatures of 18 °C (Brett 1971; Crossin et al. 2008). Increased outflow temperatures from Cultus Lake, coupled with migration earlier in the season could have detrimental impacts to the returning salmon, as high stream temperatures lead to an increase in bacteria and fungal growth as well as reductions in dissolved oxygen concentrations, impeding migration and potentially resulting in enhanced pre-spawning mortality (COSEWIC 2003). Warmer outflow temperatures could also lead to increased recreational use of the lake outlet, which may interrupt the migration of Sockeye Salmon and increase stress levels and energy use influencing subsequent mortality (Cultus Sockeye Recovery Team 2005).

Dissolved oxygen is essential for the metabolism of all aerobic aquatic species (Wetzel 2001). Dissolved oxygen concentrations decrease non-linearly with increasing water temperature (Wetzel 2001). However, the biological oxygen demand of poikilothermic species increases with increasing water temperature as their metabolic rates increase (Ficke et al. 2007). The primary sources of dissolved oxygen in a lake are through atmospheric diffusion and from photosynthesis (Kalff 2002). Oxygen is mixed throughout the lake by wind during mixis. During stratification, however, oxygen is unable to mix significantly into the hypolimnion. Increasing hypolimnetic water temperatures would therefore have a decrease in oxygen solubility and an increase in oxygen demand by fish. An *oxygen squeeze* can occur when the oxygen availability is unable to keep up with the oxygen demand of aquatic organisms (Ficke et al. 2007). It is possible that increased water temperatures from climate change would decrease the amount of oxygen available in Cultus Lake. As epilimnetic temperatures increase, another phenomenon called a *temperature-oxygen squeeze* can occur when the hypolimnetic oxygen concentrations are insufficient to keep up with fish oxygen demands and epilimnetic temperatures are too warm for sustained cold-water fish exposure (Ficke et al. 2007). As Cultus Lake shifts towards an oligomictic regime, this squeeze is expected to greatly reduce the available habitat for aquatic species forcing them into a smaller volume which in turn increases oxygen consumption, stress, and disease transmission, and reduces prey availability (Ficke et al. 2007).

The Cultus Lake Pygmy Sculpin is also expected to be affected by increased lake warming. It is presumed that the sculpin exhibits a diel vertical migration by feeding on zooplankton in the metalimnion at night and returning to depths in the day to evade predators (McPhail 2007; Woodruff and E. B. Taylor 2013). Disproportionately large amounts of energy are likely required for the Cultus Lake Pygmy Sculpin to maintain position or move vertically within the water column because it lacks a swim bladder (Woodruff and E. B. Taylor 2013). As water temperatures increase, increased energy expenditure is expected, due to reduced dissolved oxygen levels and a higher metabolic rate. A temperature-oxygen squeeze could have deleterious effects for the Cultus Lake Pygmy Sculpin as their profundal habitat becomes more hypoxic or anoxic and they are unable to persist on the lake bottom.

4.3 Trophic Status of Cultus Lake

Cultus Lake is experiencing increased nutrient loading which is leading to eutrophication. The lake has historically been oligotrophic and is presently classified as oligo-mesotrophic (Putt 2014). A shift in the algal community composition and production is expected as eutrophication continues under climate change (Vincent 2009). Cultus Lake has seen a decrease in water quality and increased presence of macrophytes and algae in recent years (Putt 2014) and an increase in primary productivity during warmer years (Shortreed 2007). In the spring, high epilimnetic nitrogen concentrations are quickly depleted as productivity increases with increased temperatures and available light (Shortreed 2007). Primary production quickly shifts to the metalimnion, owing to the high water clarity of Cultus Lake and access to hypolimnetic nutrient reserves. As there is reduced mixing in the metalimnion and upper hypolimnion, an algal community structural shift is expected, with non-motile algae likely to sediment to the bottom where they are aerobically decomposed (decreasing hypolimnetic oxygen levels), and motile algae are expected to dominate productivity (Vincent 2009). A potential shift to less nutritious algal assemblage can affect zooplankton diversity and lead to upward cascading influences in the food web for Sockeye Salmon and Cultus Lake Pygmy Sculpin. High nitrogen levels in the plunging summer baseflow from Frosst Creek (Putt 2014) will deliver additional nutrients to the metalimnion, likely sustaining continuous primary production. As the hydrological regime shifts to drier summers and wetter winters (Pacific Climate Impacts Consortium 2012), a larger portion of the summer

inflow in Frosst Creek will be expected to come from the cooler groundwater (Putt 2014), increasing metalimnetic nitrogen concentrations. Hydrological concentration of nutrients within the lake would be expected, due to decreased nutrient flushing through Sweltzer River and increased evaporation from warmer air temperatures in the summer. A longer growing season is also expected with more growing degree days as climate change continues (Pacific Climate Impacts Consortium 2012; British Columbia Ministry of Environment 2016), resulting in a higher overall algal biomass within Cultus Lake, and associated deep water decomposition. This impact could be exacerbated by expected increases in fish planktivory, and a subsequent decrease in zooplankton biomass, reducing grazing pressures on algae (B. Moss et al. 2011). However, although the nutrients in the lake would stagnate throughout the summer under climate change, projections of increased winter precipitation could both increase annual nutrient loading, but also flushing. It is unclear at this time what the net primary productivity effects of these oppositional forcings for Cultus Lake primary productivity may be, although it is likely to be a net increase in productivity.

Changes in algal community structure and function arising from increased heating and nutrient loading may create conditions where cyanobacteria dominate Cultus Lake algal communities for substantial periods of the growing season (O'Neil et al. 2012). Cyanobacteria are unicellular organisms (prokaryote) that can create large blooms rendering the water unsuitable for recreation if substantial (Paerl, Fulton, et al. 2001). Some cyanobacteria species develop hepatotoxins and neurotoxins making the water toxic for animals and humans (O'Neil et al. 2012). Dominance of the algal community by cyanobacteria can lead to an increase in toxins in the flesh of fish rendering them unsuitable for consumption (Ficke et al. 2007). Localized cyanobacteria blooms have occurred previously in Cultus Lake in 2012 (Putt 2014). More frequent cyanobacteria blooms are expected with increased nutrient loading and climate change, as certain problematic cyanobacteria thrive during long periods of stratification and enhanced epilimnetic nitrogen depletion, coupled with warm water temperatures (Ficke et al. 2007; O'Neil et al. 2012). Warm water has a reduced viscosity which is preferential for cyanobacteria that can regulate their buoyancy over larger non-motile phytoplankton that will sink in less viscous water (O'Neil et al. 2012). Certain species of cyanobacteria would therefore have a competitive advantage to access nutrients trapped in the hypolimnion (O'Neil et al. 2012), particularly in Cultus Lake, since light can penetrate deeper than the thermocline. Another selective advantage heterocystous cyanobacteria have in periods of long stratification is their ability to survive in nitrogen-limited conditions

through fixation of atmospheric nitrogen (Paerl, Fulton, et al. 2001; Ficke et al. 2007; O'Neil et al. 2012). However, the formation of large cyanobacterial mats on the lake surface under nitrogen-limitation could create shading effects further limiting deep water productivity and out-competing other algal species (Paerl and Huisman 2009), but generally leading to the degradation of water quality and food webs for species at risk.

The propagation of invasive Eurasian watermilfoil (*Myriophyllum spicatum L.*, EWM) increases with eutrophication (C. S. Smith and Barko 1990). EWM was first observed in Cultus Lake in 1977 (Mossop and Bradford 2004). Growth rates of EWM increase with increasing water temperatures: a maximum growth rate occurs at relatively high water temperatures (30 °C–35 °C) (C. S. Smith and Barko 1990). In high clarity lakes, such as Cultus Lake, EWM is able to grow at greater depths, increasing its footprint and potentially expanding its coverage to all littoral regions of the lake. EWM grows rapidly and tends to form canopies or mats, often extending to the water surface. Increased growth of EWM can increase the rate of eutrophication because of their access to phosphorus sequestered in the sediments. Sequestering of sediment-bound phosphorus is the primary uptake pathway for EWM (C. S. Smith and Barko 1990; Ficke et al. 2007). Upon dying, this phosphorus that was otherwise unavailable to other producers in the lake is released into the water column where it can stimulate algae growth and further growth of EWM and other macrophytes (C. S. Smith and Barko 1990; Ficke et al. 2007), in addition to the depletion of hypolimnetic dissolved oxygen concentrations as bacteria aerobically decompose the organic matter (Kankaala et al. 2002). Additionally, salmonids are particularly affected by EWM invasions because of the growth of EWM in spawning grounds (C. S. Smith and Barko 1990; Mossop and Bradford 2004; Ficke et al. 2007). EWM colonies may also provide habitat for juvenile Northern Pikeminnow (*Ptychocheilus oregonensis*); adult Northern Pikeminnow are a natural predator of Sockeye Salmon. It has been hypothesized that EWM provides shelter for juvenile Northern Pikeminnow from being cannibalistic prey of adult Northern Pikeminnow (Mossop and Bradford 2004). So, an increase in survival for juvenile Northern Pikeminnow could mean an increased predation of juvenile Sockeye Salmon. It has also been speculated that increased refuge for Northern Pikeminnow could increase predation on Cultus Lake Pygmy Sculpin (COSEWIC 2010).

4.4 Managing the Impacts of Climate Change

A changing climate cannot be ameliorated at the regional level and requires global participation. However, given the interactivity of climate warming and eutrophication on lake ecosystems (B. Moss et al. 2011), regional nutrient mitigation measures can be undertaken to reduce the impacts of climate change on Cultus Lake to protect Sockeye Salmon and Cultus Lake Pygmy Sculpin. As watershed loading of nitrogen to Cultus Lake is elevated from atmospheric and landscape sources, Putt (2014) recommends targeting phosphorus to mitigate eutrophication trajectories in Cultus Lake. Heavy septic usage in the summer may be leading to high phosphorus loading in Cultus Lake (Putt 2014). Water quality may be improved by limiting nutrient inputs by modifying sewage disposal. Additionally, migratory gulls overnighting in Cultus Lake during the fall-through-spring period has led to a rise in phosphorus loadings from guano (Putt 2014). Non-lethal mitigation methods may be employed in regional agricultural areas to reduce the number of gulls returning to Cultus Lake (Cook et al. 2008). Finally, agriculture in the Frosst Creek watershed represents a large source of nutrients for Cultus Lake (Putt 2014). Care should be taken to alter agricultural management practices to reduce nutrient runoff, especially with an expected change in hydrological regime. The application of these phosphorus mitigation strategies would likely reduce the effects of eutrophication on Cultus Lake, making the system less reactive to climate change over the next century.

Chapter 5

Conclusions

Climate change and accelerated eutrophication are threatening the habitat for at-risk species and affecting the water quality in Cultus Lake. The total lake heat content has increased since the early 20th century and is projected to accelerate through the 21st century under climate change scenarios RCP4.5 and RCP8.5. Similarly, the stability and intensity of stratification of the lake has historically been increasing, and is expected to continue increasing through 2100 under the two climate change scenarios explored. Along with an increase in stratification strength, Cultus Lake is remaining stratified for a longer period. The onset of summer stratification is expected to continue occurring in late March and early April, while the breakup of stratification is expected to occur later, shifting from early December to mid to late January with some years remaining stratified throughout the winter. These projections suggest the lake is shifting from a warm monomictic regime toward an oligomictic regime. Reduced winter whole-lake mixing would therefore reduce the amount of hypolimnetic dissolved oxygen, thus threatening the available habitat for cold-water species. Finally, surface and outflow temperatures during the Sockeye Salmon run (August–November) have also been increasing with climate change. Surface temperatures have a direct response to air temperatures (Adrian et al. 2009), indicating that air temperatures have been increasing since the early 20th century. Surface and outflow temperatures during late summer and the fall are projected to increase at a higher rate in the future. Increased water temperatures can accelerate the effects of eutrophication, such as more frequent cyanobacteria blooms, which owing to their enhanced organic matter production, could accelerate annual hypolimnetic water oxygen depletion.

It is important that first-order lake stresses that are interactive with climate change, such as eutrophication, are minimized to reduce the impacts of climate change on Cultus Lake and its species-at-risk. Regional measures can be undertaken to abate nutrient inputs into Cultus Lake to reduce or reverse eutrophication. It is recommended that further investigation of the interactive effects of climate change and eutrophication on Cultus Lake be conducted by coupling this physical lake model with a suite of biogeochem-

ical models, such as AED or CAEDYM (Hipsey and Hamilton 2008). Such an approach will likely afford quantitative insight on future lake outcomes, to inform lake and watershed management and improve outcomes for Cultus Lake and its species-at-risk.

References

Adrian, Rita, Catherine M. O'Reilly, Horacio Zagarese, Stephen B. Baines, Dag O. Hessen, Wendel Keller, David M. Livingstone, Ruben Sommaruga, Dietmar Straile, Ellen Van Donk, et al. (2009). "Lakes as sentinels of climate change". In: *Limnology and oceanography* 54.6, p. 2283. DOI: 10.4319/lo.2009.54.6_part_2.2283.

AERONET (2017). *Aerosol Robotic Network: Saturna Island*. URL: https://aeronet.gsfc.nasa.gov/cgi-bin/type_one_station_opera_v2_new?site=Saturn_Island&nachal=2&level=3&place_code=10 (visited on 03/29/2017).

Anderson, Donald M., Patricia M. Glibert, and Joann M. Burkholder (2002). "Harmful algal blooms and eutrophication: nutrient sources, composition, and consequences". In: *Estuaries* 25.4, pp. 704–726. DOI: 10.1007/bf02804901.

Arora, V. K., J. F. Scinocca, G. J. Boer, J. R. Christian, K. L. Denman, G. M. Flato, V. V. Kharin, W. G. Lee, and W. J. Merryfield (2011). "Carbon emission limits required to satisfy future representative concentration pathways of greenhouse gases". In: *Geophysical Research Letters* 38.5. DOI: 10.1029/2010GL046270.

Barry, Roger G. and Richard J. Chorley (1976). *Atmosphere, weather, and climate*. English. 3d. Vol. 208. London: Methuen Publishing Ltd. ISBN: 0416704204.

Bartsch, A. F. (1970). "Accelerated eutrophication of lakes in the United States: ecological response to human activities". In: *Environmental Pollution (1970)* 1.2, pp. 133–140. DOI: 10.1016/0013-9327(70)90013-3.

Bird, R. E. and R. L. Hulstrom (1981). *Simplified clear sky model for direct and diffuse insolation on horizontal surfaces*. Tech. rep. Solar Research Institute. DOI: 10.2172/6510849.

Brett, John R. (1971). "Energetic responses of salmon to temperature. A study of some thermal relations in the physiology and freshwater ecology of sockeye salmon (Oncorhynchus nerka)". In: *American Zoologist* 11 (11), pp. 99–113. DOI: 10.1093/icb/11.1.99.

British Columbia Ministry of Environment (2016). *Indicators of Climate Change for British Columbia: 2016 Update*. Ed. by Thomas White, Johanna Wolf, Faron Anslow, Arelia Werner, and Reber Creative. ISBN: 0-7726-4732-1.

Britton, C. M. and J. D. Dodd (1976). "Relationships of photosynthetically active radiation and shortwave irradiance". In: *Agricultural Meteorology* 17.1, pp. 1–7. DOI: 10.1016/0002-1571(76)90080-7.

Campolongo, Francesca, Jessica Cariboni, and Andrea Saltelli (2007). "An effective screening design for sensitivity analysis of large models". In: *Environmental modelling & software* 22.10, pp. 1509–1518. DOI: 10.1016/j.envsoft.2006.10.004.

Chambers, P. A., M. Guy, E. S. Roberts, M. N. Charlton, R. Kent, C. Gagnon, G. Grove, and N. Foster (2001). "Nutrients and their impact on the Canadian environment". In: *Agriculture and Agri-Food Canada, Environment Canada, Fisheries and Oceans Canada, Health Canada and Natural Resources Canada*, p. 241.

Chiang, E., L. Pon, D. T. Selbie, J. M. B. Hume, P. Woodruff, and G. Velema (2015). "Identification of critical habitat for Coastrange Sculpin (Cultus Population)(Cottus aleuticus)". In: *DFO Canadian Science Advisory Secretariat Research Document* 33.

Christensen, Michael R., Mark D. Graham, Rolf D. Vinebrooke, David L. Findlay, Michael J. Paterson, and Michael A. Turner (2006). "Multiple anthropogenic stressors cause ecological surprises in boreal lakes". In: *Global Change Biology* 12.12, pp. 2316–2322. DOI: 10.1111/j.1365-2486.2006.01257.x.

Christian, J. R., V. K. Arora, G. J. Boer, C. L. Curry, K. Zahariev, K. L. Denman, G. M. Flato, W. G. Lee, W. J. Merryfield, N. T. Roulet, and J. F. Scinocca (2010). "The global carbon cycle in the Canadian Earth system model (CanESM1): Preindustrial control simulation". In: *Journal of Geophysical Research: Biogeosciences* 115. DOI: 10.1029/2008JG000920.

Clark, Colin W. and David A. Levy (1988). "Diel Vertical Migrations by Juvenile Sockeye Salmon and the Antipredation Window". In: *The American Naturalist* 131.2, pp. 271–290. DOI: 10.1086/284789.

Cook, Aonghais, Steven Rushton, John Allan, and Andrew Baxter (2008). "An Evaluation of Techniques to Control Problem Bird Species on Landfill Sites". In: *Environmental Management* 41.6, pp. 834–843. DOI: 10.1007/s00267-008-9077-7.

Cooke, Steven J., Scott G. Hinch, Anthony P. Farrell, Michael F. Lapointe, Simon R. M. Jones, J. Steveson Macdonald, David A. Patterson, Michael

C. Healey, and Glen Van Der Kraak (2004). "Abnormal Migration Timing and High en route Mortality of Sockeye Salmon in the Fraser River, British Columbia". In: *Fisheries* 29.2, pp. 22–33. DOI: 10.1577/1548-8446(2004)29[22:AMTAHE]2.0.CO;2.

COSEWIC (2003). *COSEWIC Assessment and Status Report on the Sockeye Salmon Oncorhynchus nerka, Cultus population in Canada*. Tech. rep. Ottawa: Committee on the Status of Endangered Wildlife in Canada. URL: http://www.registrelep-sararegistry.gc.ca/virtual_sara/files/cosewic/sr%5Fcultus%5Fsockeye%5Fsalmon%5Fe%2Epdf (visited on 10/13/2016).

— (2010). *COSEWIC Assessment and Status Report on the Coastrange Sculpin Cottus aleuticus, Cultus Population in Canada*. Tech. rep. Ottawa: Committee on the Status of Endangered Wildlife in Canada. URL: http://www.registrelep-sararegistry.gc.ca/virtual_sara/files/cosewic/sr%5FCoastrange%20Sculpin%5F0810%5Fe1%2Epdf (visited on 10/13/2016).

Crossin, Glenn Terrence, S. G. Hinch, S. J. Cooke, D. W. Welch, D. A. Patterson, S. R. M. Jones, A. G. Lotto, R. A. Leggatt, M. T. Mathes, J. M. Shrimpton, G. Van Der Kraak, and A. P. Farrell (2008). "Exposure to high temperature influences the behaviour, physiology, and survival of sockeye salmon during spawning migration". In: *Canadian Journal of Zoology* 86.2, pp. 127–140. DOI: 10.1139/Z07-122.

Crozier, L. G., A. P. Hendry, P. W. Lawson, T. P. Quinn, N. J. Mantua, J. Battin, R. G. Shaw, and R. B. Huey (2008). "Potential responses to climate change in organisms with complex life histories: evolution and plasticity in Pacific salmon". In: *Evolutionary Applications* 1.2, pp. 252–270. DOI: 10.1111/j.1752-4571.2008.00033.x.

Cultus Sockeye Recovery Team (2005). *National conservation strategy for the sockeye salmon, (Oncorhynchus nerka), Cultus Lake population, in British Columbia*. Tech. rep. Fisheries and Oceans Canada. URL: http://www.dfo-mpo.gc.ca/Library/334716.pdf (visited on 11/16/2016).

Delcan (2012). *Cultus Lake Traffic and Transportation Study*. Tech. rep. Vancouver: Delcan Corporation.

Dera, Jerzy and Howard R. Gordon (1968). "Light field fluctuations in the photic zone". In: *Limnology and Oceanography* 13.4, pp. 697–699.

Engelhardt, Christof and Georgiy Kirillin (2014). "Criteria for the onset and breakup of summer lake stratification based on routine temperature measurements". In: *Fundamental and Applied Limnology/Archiv für Hydrobiologie* 184.3, pp. 183–194. DOI: 10.1127/1863-9135/2014/0582.

Environment and Climate Change Canada (2017). *Canadian regional climate model*. Government of Canada. URL: http://www.ec.gc.ca/ccmac-cccma/default.asp?lang=En&n=7CC1E8B6-1 (visited on 06/26/2017).

Environment and Natural Resources Canada (2017). *Engineering Climate Datasets: Canadian Weather Energy and Engineering Datasets (CWEEDS)*. Government of Canada. URL: http://climate.weather.gc.ca/prods_servs/engineering_e.html (visited on 06/26/2017).

Environmental Reporting BC (2015). *Status of Ground-Level Ozone in B.C. (2011-2013)*. Tech. rep. Government of British Columbia: Ministry of Environment. URL: http://www.env.gov.bc.ca/soe/indicators/air/print_ver/envreportbc_ozone_August2015.pdf (visited on 03/29/2017).

Ficke, Ashley D., Christopher A. Myrick, and Lara J. Hansen (2007). "Potential impacts of global climate change on freshwater fisheries". In: *Reviews in Fish Biology and Fisheries* 17.4, pp. 581–613. DOI: 10.1007/s11160-007-9059-5.

Fisher, Hugo B., E. John List, Robert C.Y. Koh, Joerg Imberger, and Norman H. Brooks (1979). *Mixing in Inland and Coastal Waters*. Academic Press. 302 pp. ISBN: 0122581504.

Flato, G., J. Marotzke, B. Abiodun, P. Braconnot, S. C. Chou, W. Collins, P. Cox, F. Driouech, S. Emori, V. Eyring, C. Forest, P. Gleckler, E. Guilyardi, C. Jakob, V. Kattsov, C. Reason, and M. Rummukain (2013). "Evaluation of Climate Models". In: *Climate Change 2013: The Physical Science Basis: Working Group I Contribution to the Fifth Assessment Report of the Intergovernmental Panel on Climate Change*. Cambridge University Press, pp. 741–866. DOI: 10.1017/CBO9781107415324.020.

Foerster, R. E. (1925). "Studies in the ecology of the sockeye salmon (Oncorhynchus nerka)". In: *Contributions to Canadian Biology* 2, p. 335.

George, Glen, Margaret Hurley, and Dian Hewitt (2007). "The impact of climate change on the physical characteristics of the larger lakes in the English Lake District". In: *Freshwater Biology* 52.9, pp. 1647–1666. DOI: 10.1111/j.1365-2427.2007.01773.x.

Gerten, Dieter and Rita Adrian (2001). "Differences in the persistency of the North Atlantic Oscillation signal among lakes". In: *Limnology and Oceanography* 46.2, pp. 448–455. DOI: 10.4319/lo.2001.46.2.0448.

Goodlad, J. C., T. W. Gjernes, and E. L. Brannon (1974). "Factors affecting sockeye salmon (Oncorhynchus nerka) growth in four lakes of the Fraser River system". In: *Journal of the Fisheries Board of Canada* 31.5, pp. 871–892. DOI: 10.1139/f74-106.

Gutowski Jr, William J., Steven G. Decker, Rodney A. Donavon, Zaitao Pan, Raymond W. Arritt, and Eugene S. Takle (2003). "Temporal–spatial scales of observed and simulated precipitation in central US climate". In: *Journal of Climate* 16.22, pp. 3841–3847. DOI: 10.1175/1520-0442(2003)016<3841:TSOOAS>2.0.CO;2.

Healey, Michael (2011). "The cumulative impacts of climate change on Fraser River sockeye salmon (Oncorhynchus nerka) and implications for management". In: *Canadian Journal of Fisheries and Aquatic Sciences* 68.4, pp. 718–737. DOI: 10.1139/f2011-010.

Hipsey, M. R., L. C. Bruce, and D. P. Hamilton (2013). *Aquatic Ecodynamics (AED) Model Library Science Manual*.

— (2014). *General Lake Model: Model Overview and User Information; v 2.0β*. URL: http://aed.see.uwa.edu.au/research/models/GLM/downloads/AED_GLM_v2_0b0_20141025.pdf (visited on 09/21/2016).

Hipsey, M. R. and D. P. Hamilton (2008). "Computational aquatic ecosystem dynamics model: CAEDYM v3, Science Manual". In: *University of Western Australia*.

Holding, S. and Diana A. (2012). *Cultus Lake Watershed Numerical Groundwater Flow Model*. Tech. rep. Department of Earth Sciences Simon Fraser University. URL: https://www.psf.ca/sites/default/files/FSWP_11_34_FR_Attachment_Cultus_Lake_Groundwater_Model_Report.pdf (visited on 11/01/2016).

Idso, Sherwood B. (1973). "On the concept of lake stability". In: *Limnology and Oceanography* 18.4, pp. 681–683. DOI: 10.4319/lo.1973.18.4.0681.

Imberger, J. and J. C. Patterson (1981). "Dynamic Reservoir Simulation Model- DYRESM: 5". In: *Transport Models for Inland and Coastal Waters*. New York: Academic Press.

Imboden, Dieter M. and Alfred Wüest (1995). *Mixing mechanisms in lakes*. In: *Physics and chemistry of lakes*. Springer, pp. 83–138.

Instruments, Swoffer (2016). *Swoffer Instruments Inc. Model 3000 Current M eter Flow Calculator: Data Recorder*. URL: http://www.swoffer.com/pdf/3000bulet16.pdf (visited on 02/14/2017).

IOC, SCOR (2010). *IAPSO: The international thermodynamic equation of seawater–2010: Calculation and use of thermodynamic properties, Intergovernmental Oceanographic Commission, Manuals and Guides No. 56*, p. 196.

IPCC (2013). *Climate Change 2013: The Physical Science Basis. Contribution of Working Group I to the Fifth Assessment Report of the Intergovernmental Panel on Climate Change*. Ed. by T. F. Stocker, D. Qin,

G. K. Plattner, M. Tignor, S. K. Allen, J. Boschung, A. Nauels, Y. Xia, V. Bex, and P. M. Midgley. Cambridge, United Kingdom and New York, NY, USA: Cambridge University Press, p. 1535.

ISO (2010). *ISO 1100-2:2010 Hydrometry – Measurement of liquid flow in open channels – Part 2: Determination of the stage-discharge relationship*. Tech. rep. Geneva, Switzerland: International Organization for Standardization.

Jeppesen, Erik, Brian Moss, Helen Bennion, Laurence Carvalho, Luc De Meester, Heidrun Feuchtmayr, Nikolai Friberg, Mark O. Gessner, Mariet Hefting, Torben L. Lauridsen, Lone Liboriussen, Hilmar J. Malmquist, Linda May, Mariana Meerhoff, Jon S. Olafsson, Merel B. Soons, and Jos T. A. Verhoeven (2010). "Interaction of Climate Change and Eutrophication". In: *Climate Change Impacts on Freshwater Ecosystems*. Ed. by Martin Kernan, Richard W. Battarbee, and Brian Moss. Blackwell Publishing, Oxford. Chap. 6, pp. 119–151. DOI: 10.1002/9781444327397.ch6.

Kalff, Jacob (2002). *Limnology: inland water ecosystems*. Vol. 592. Prentice Hall New Jersey.

Kankaala, Paula, Anne Ojala, Tiina Tulonen, and Lauri Arvola (2002). "Changes in nutrient retention capacity of boreal aquatic ecosystems under climate warming: a simulation study". In: *Hydrobiologia* 469.1, pp. 67–76. DOI: 10.1023/A:1015563224554.

Kraemer, Benjamin M., Orlane Anneville, Sudeep Chandra, Margaret Dix, Esko Kuusisto, David M. Livingstone, Alon Rimmer, S. Geoffrey Schladow, Eugene Silow, Lewis M. Sitoki, Rashid Tamatamah, Yvonne Vadeboncoeur, and Peter B. McIntyre (2015). "Morphometry and average temperature affect lake stratification responses to climate change". In: *Geophysical Research Letters* 42.12, pp. 4981–4988. DOI: 10.1002/2015GL064097.

Levy, David A. (1990). "Reciprocal Diel Vertical Migration Behavior in Planktivores and Zooplankton in British Columbia Lakes". In: *Canadian Journal of Fisheries and Aquatic Sciences* 47.9, pp. 1755–1764. DOI: 10.1139/f90-199.

Lewis, William M. (1979). *Zooplankton Community Analysis*. Springer New York. DOI: 10.1007/978-1-4612-9986-8.

Livingstone, David M. (2008). "A change of climate provokes a change of paradigm: taking leave of two tacit assumptions about physical lake forcing". In: *International Review of Hydrobiology* 93.4-5, pp. 404–414. DOI: 10.1002/iroh.200811061.

Matzinger, Andreas, Martin Schmid, Elizabeta Veljanoska-Sarafiloska, Suzana Patceva, Dafina Guseska, Bernd Wagner, Beat Müller, Michael Sturm, and Alfred Wüest (2007). "Eutrophication of ancient Lake Ohrid: Global warming amplifies detrimental effects of increased nutrient inputs". In: *Limnology and Oceanography* 52.1, pp. 338–353. DOI: 10.4319/lo.2007.52.1.0338.

McGinley, Paul M., Kevin C. Masarik, Madeline B. Gotkowitz, and David J. Mechenich (2016). "Impact of anthropogenic geochemical change and aquifer geology on groundwater phosphorus concentrations". In: *Applied Geochemistry* 72, pp. 1–9. DOI: http://dx.doi.org/10.1016/j.apgeochem.2016.05.020.

McPhail, John Donald (2007). *The freshwater fishes of British Columbia*. University of Alberta.

Moss, Brian, Sarian Kosten, Mariana Meerhoff, Richard W. Battarbee, Erik Jeppesen, Néstor Mazzeo, Karl Havens, Gissell Lacerot, Zhengwen Liu, Luc De Meester, Hans Paerl, and Marten Scheffer (2011). "Allied attack: climate change and eutrophication". In: *Inland Waters* 1.2, pp. 101–105. DOI: 10.5268/IW-1.2.359.

Moss, Richard H., Jae A. Edmonds, Kathy A. Hibbard, Martin R. Manning, Steven K. Rose, Detlef P. Van Vuuren, Timothy R. Carter, Seita Emori, Mikiko Kainuma, Tom Kram, Gerald A. Meehl, John F. B. Mitchell, Nebojsa Nakicenovic, Keywan Riahi, Steven J. Smith, Ronald J. Stouffer, Allison M. Thomson, John P. Weyant, and Thomas J. Wilbanks (2010). "The next generation of scenarios for climate change research and assessment". In: *Nature* 463.7282, pp. 747–756. DOI: 10.1038/nature08823.

Mossop, Brent and Michael J. Bradford (2004). *Review of Eurasian watermilfoil control at Cultus Lake and recommendations for future removals*. Tech. rep. Fisheries and Oceans Canada Fraser River Stock Assessment.

O'Neil, J. M., T. W. Davis, M. A. Burford, and C. J. Gobler (2012). "The rise of harmful cyanobacteria blooms: The potential roles of eutrophication and climate change". In: *Harmful Algae* 14, pp. 313–334. DOI: 10.1016/j.hal.2011.10.027.

Onset Computer Corporation (2008). *Wind Speed/Direction Smart Sensor (S-WCA-M003) Manual*. URL: http://www.onsetcomp.com/files/manual_pdfs/6858-G-MAN-S-WCA.pdf (visited on 04/06/2017).

— (2017a). *Barometric Pressure Smart Sensor (S-BPA-CM10) Manual*. URL: http://www.onsetcomp.com/files/manual_pdfs/6122-E%20MAN-S-BPA.pdf (visited on 04/06/2017).

Onset Computer Corporation (2017b). *HOBO U20 Water Level Logger (U20-001-0x and U20-001-0x-Ti) Manual*. URL: http://www.onsetcomp.com/files/manual_pdfs/12315-H%20MAN-U20.pdf (visited on 03/01/2017).

— (2017c). *TidbiT v2 Temp (UTBI-001) Manual*. URL: http://www.onsetcomp.com/files/manual_pdfs/10385-H%20MAN-UTBI-001.pdf (visited on 03/01/2017).

O'Reilly, Catherine M. et al. (2015). "Rapid and highly variable warming of lake surface waters around the globe". In: *Geophysical Research Letters* 42.24, pp. 10, 773–10, 781. DOI: 10.1002/2015GL066235.

Pacific Climate Impacts Consortium (2012). *Plan2Adapt*. URL: https://plan2adapt.ca (visited on 07/13/2017).

Paerl, Hans W., Rolland S. Fulton, Pia H. Moisander, and Julianne Dyble (2001). "Harmful freshwater algal blooms, with an emphasis on cyanobacteria". In: *The Scientific World Journal* 1, pp. 76–113. DOI: 10.1100/tsw.2001.16.

Paerl, Hans W. and J. Huisman (2009). "Climate change: a catalyst for global expansion of harmful cyanobacterial blooms". In: *Environmental Microbiology Reports* 1 (1), pp. 27–37. DOI: 10.1111/j.1758-2229.2008.00004.x.

Panofsky, Hans A. and Glenn W. Brier (1958). *Some Application of Statistics to Meteorology*. University Park, Pennsylvania: College of Mineral Industries, Pennsylvania State University.

Pörtner, Hans O. and Anthony P. Farrell (2008). "Physiology and Climate Change". In: *Science* 322.5902, pp. 690–692.

Putt, Annika Elsie (2014). "Spatiotemporal nutrient loading to Cultus Lake: Context for eutrophication and implications for integrated watershed-lake management". MA thesis. Simon Fraser University. URL: http://rem-main.rem.sfu.ca/theses/PuttAnnika_2014_MRM591.pdf (visited on 05/02/2016).

Reynolds, C. S. (2009). "Biological–Physical Interactions". In: *Encyclopedia of Inland Waters*. Ed. by Gene E Likens. Vol. 1, pp. 515–521.

Ricker, William E. (1937). "Physical and Chemical Characteristics of Cultus Lake, British Columbia." In: *Journal of the Biological Board of Canada* 3.4, pp. 363–402. DOI: 10.1139/f37-022.

Robertson, Dale M. and William J. Rose (2011). "Response in the trophic state of stratified lakes to changes in hydrology and water level: potential effects of climate change". In: *Journal of Water and Climate Change* 2.1, pp. 1–18. DOI: 10.2166/wcc.2011.026.

Sahoo, G. B., A. L. Forrest, S. G. Schladow, J. E. Reuter, R. Coats, and M. Dettinger (2015). "Climate change impacts on lake thermal dynamics and ecosystem vulnerabilities". In: *Limnology and Oceanography* 61.2, pp. 496–507. DOI: 10.1002/lno.10228.

SARA (2002). "Species at Risk Act. SC 2002, c 29". In: URL: http://laws-lois.justice.gc.ca/PDF/S-15.3.pdf (visited on 08/09/2017).

Schelker, Jakob, Karin Öhman, Stefan Löfgren, and Hjalmar Laudon (2014). "Scaling of increased dissolved organic carbon inputs by forest clear-cutting–What arrives downstream?" In: *Journal of hydrology* 508, pp. 299–306. DOI: 10.1016/j.jhydrol.2013.09.056.

Scheuerell, Mark D. and Daniel E. Schindler (2003). "Diel vertical migration by juvenile sockeye salmon: empirical evidence for the antipredation window". In: *Ecology* 84.7, pp. 1713–1720. DOI: 10.1890/0012-9658(2003)084[1713:DVMBJS]2.0.CO;2.

Schindler, Daniel E., Donald E. Rogers, Mark D. Scheuerell, and Caryn A. Abrey (2005). "Effects of changing climate on zooplankton and juvenile sockeye salmon growth in southwestern Alaska". In: *Ecology* 86.1, pp. 198–209. DOI: 10.1890/03-0408.

Schindler, David W. (2012). "The dilemma of controlling cultural eutrophication of lakes". In: *Proceedings of the Royal Society B: Biological Sciences*. The Royal Society. DOI: 10.1098/rspb.2012.1032.

Scibek, J. and D. Allen (2006). "Comparing modelled responses of two high-permeability, unconfined aquifers to predicted climate change". In: *Global and Planetary Change* 50.1-2, pp. 50–62. DOI: 10.1016/j.gloplacha.2005.10.002.

Scinocca, J. F., V. V. Kharin, Y. Jiao, M. W. Qian, M. Lazare, L. Solheim, G. M. Flato, S. Biner, M. Desgagne, and B. Dugas (2016). "Coordinated Global and Regional Climate Modeling". In: *Journal of Climate* 29.1, pp. 17–35. DOI: 10.1175/JCLI-D-15-0161.1.

Seabird Scientific (2016a). *SBE 19plus V2 SeaCAT Profiler CTD User Manual: Conductivity, Temperature, & Pressure Recorder with RS-232 Interface*.

— (2016b). *Seasoft V2: SBE Data Processing Software Manual*. URL: http://www.seabird.com/sites/default/files/documents/SBEDataProcessing_7.26.4.pdf (visited on 04/12/2017).

Shortreed, K. R. S. (2007). *Limnology of Cultus Lake, British Columbia*. Tech. rep. Fisheries and Oceans Canada.

Smith, Craig S. and J. W. Barko (1990). "Ecology of Eurasian watermilfoil." In: *Journal of Aquatic Plant Management* 28.2, pp. 55–64.

Smith, Val H. and David W. Schindler (2009). "Eutrophication science: where do we go from here?" In: *Trends in ecology & evolution* 24.4, pp. 201–207.

Søndergaard, Martin, Jens Peder Jensen, and Erik Jeppesen (2003). "Role of sediment and internal loading of phosphorus in shallow lakes". In: *Hydrobiologia* 506.1, pp. 135–145. DOI: 10.1023/B:HYDR.0000008611.12704.dd.

Stainsby, E. A., J. G. Winter, H. Jarjanazi, A. M. Paterson, D. O. Evans, and J. D. Young (2011). "Changes in the thermal stability of Lake Simcoe from 1980 to 2008". In: *Journal of Great Lakes Research* 37, pp. 55–62. DOI: 10.1016/j.jglr.2011.04.001.

Stefan, Heinz G. and Eric B. Preud'homme (1993). "Stream temperature estimation from air temperature". In: *Journal of the American Water Resources Association* 29.1, pp. 27–45.

Stull, Roland (2015). *Practical Meteorology: An Algebra-based Survey of Atmospheric Science*. University of British Columbia. ISBN: 978-0-88865-176-1. URL: https://www.eoas.ubc.ca/books/Practical_Meteorology/prmet/PracticalMet_WholeBook-v1_00b.pdf (visited on 02/21/2017).

Taylor, Karl E., Ronald J. Stouffer, and Gerald A. Meehl (2012). "An Overview of CMIP5 and the Experiment Design". In: *Bulletin of the American Meteorological Society* 93.4, pp. 485–498. DOI: 10.1175/BAMS-D-11-00094.1.

Trimble, Sabina (2016). "Storying Swí:lhcha: Place Making and Power at a Stó:lō Landmark". In: *BC Studies* 190, p. 39. URL: http://ojs.library.ubc.ca/index.php/bcstudies/article/viewFile/187241/186087 (visited on 05/02/2017).

UNESCO (1981). *Tenth report of the joint panel on oceanographic tables and standards*. URL: http://unesdoc.unesco.org/images/0004/000461/046148eb.pdf (visited on 11/18/2016).

Vallentyne, John R. (1974). *The Algal Bowl: Lakes and Man*. Dept. of the Environment, Fisheries and Marine Service.

Vincent, W. F. (2009). "Effects of Climate Change on Lakes". In: *Encyclopedia of Inland Waters*. Ed. by Gene E Likens. Vol. 3, pp. 55–60.

von Salzen, Knut, John F. Scinocca, Norman A. McFarlane, Jiangnan Li, Jason N. S. Cole, David Plummer, Diana Verseghy, M. Cathy Reader, Xiaoyan Ma, Michael Lazare, and Larry Solheim (2013). "The Canadian Fourth Generation Atmospheric Global Climate Model (CanAM4). Part I: Representation of Physical Processes". In: *Atmosphere-Ocean* 51.1, pp. 104–125. DOI: 10.1080/07055900.2012.755610.

Weinberger, Stefan and Mark Vetter (2014). "Lake heat content and stability variation due to climate change: coupled regional climate model (REMO)-lake model (DYRESM) analysis". In: *Journal of Limnology* 73.1. DOI: 10.4081/jlimnol.2014.668.

Wetzel, Robert G. (2001). *Limnology: lake and river ecosystems*. 3rd. Academic Press. ISBN: 0127447601.

Wieringa, Jon (1992). "Updating the Davenport roughness classification". In: *Journal of Wind Engineering and Industrial Aerodynamics* 41.1-3, pp. 357–368. DOI: 10.1016/0167-6105(92)90434-c.

Woodruff, Patricia E. and Eric B. Taylor (2013). "Assessing the distinctiveness of the Cultus pygmy sculpin, a threatened endemic, from the widespread coastrange sculpin Cottus aleuticus". In: *Endangered Species Research* 20.2, pp. 181–194. DOI: 10.3354/esr00493.

Yajima, Hiroshi and Shigetomo Yamamoto (2015). "Improvements of Radiation Estimations for a Simulation of Water Temperature in a Reservoir". In: *Journal of Japan Society of Civil Engineers, Ser. B1 (Hydraulic Engineering)* 71.4. DOI: 10.2208/jscejhe.71.i_775.

Zubel, Marc (2000). *Groundwater Conditions of the Columbia Valley Aquifer Cultus Lake , British Columbia*. Tech. rep. Ministry of Environment, Lands & Parks, p. 98. URL: http://a100.gov.bc.ca/appsdata/acat/documents/r6477/1287_1143682706883_8b7182b483ed458aad9da29ff7cef555.pdf (visited on 11/01/2016).

Appendix A

Inflow and Outflow Descriptions

Hydrological and morphological characteristics of the three largest streams from the Cultus Lake watershed are described in detail: Frosst Creek, Watt Creek, and Smith Falls Creek.

Frosst Creek is the main inflow to Cultus Lake, entering at the south end of the lake, north of Lindell Beach. Frosst Creek flows from the forested region around the United States border into the Columbia Valley which is predominantly developed for agriculture. The downstream stream course was diverted from the middle of Lindell Beach northward to its present course around the 1940s (Cultus Sockeye Recovery Team 2005). Water Survey of Canada (WSC) gauge 08MH072 (Frosst Creek near Lindell Beach) located near the Columbia Valley Highway bridge regularly recorded flow rates between 1960 and 1964. The drainage area is approximately 36 km^2. The upper reaches of the stream are fairly steep with a gradient of 12 % and decreasing to 4 % near the mouth (Zubel 2000). The bankfull discharge, or two-year flood return, is approximately 8.5 $m^3 s^{-1}$ based on a log-Pearson Type III distribution for the WSC data with annual extremes typically occurring in November and December. At the 2016 gauging location, the stream morphology consists of rapids and pools, with measurements being taken in a pool. The width and maximum depth at the gauging location were 6.2 m and 0.82 m, respectively at high flow on 16 November. A summer baseflow was found to be 0.2 $m^3 s^{-1}$. The D_{50} grain size is estimated at 70 mm, but large boulders measuring 300 mm–500 mm are present. The presence of large boulders and the steep slope indicate that Frosst Creek is capable of moving large volumes of water at great force.

Watt Creek is an intermittent creek, drying in the summer during periods of low precipitation. The creek mouth is located east of Lindell Beach. The drainage area is 6.6 km^2 (Putt 2014) and consists predominantly of forested areas from Cultus Lake Provincial Park. Upstream of the Columbia Valley Highway bridge, the slope is relatively mild because a log weir is installed at the foot of the bridge to prevent scouring of the foundations. The stream

undergoes a series of falls downstream of the log weir before leveling out prior to entering Cultus Lake. The width of the creek at the gauging location was 2.5 m and the maximum depth was 0.3 m at a discharge of 0.2 $m^3 s^{-1}$ on 16 November 2016. The bed material ranges from gravel to small cobble with the presence of some large rocks. Watt Creek is expected to have flashy flow characteristics due to the small drainage area and steep slopes.

Smith Falls Creek is a perennial stream that enters Cultus Lake at the northeast shore with a drainage area of 6.5 km^2. Smith Falls Creek has two arms: the southern arm is situated in Cultus Lake Provincial Park, the northern arm consists of wetlands created in the flat topography which likely is the result of the summer baseflow of 0.03 $m^3 s^{-1}$. The creek consists of many chutes and pools. A waterfall (Smith Falls) is located immediately upstream of the Columbia Valley Highway where the stream enters a culvert that flows to the mouth at Cultus Lake. At the stream gauging station, the creek had a width of 2.7 m and a maximum depth of 0.4 m with a discharge of 0.3 $m^3 s^{-1}$ on 16 November. The bed material consists of sand ranging to large gravel. Similarly to Watt Creek, Smith Falls Creek likely has flashy flows.

Sweltzer River is the only outlet of Cultus Lake. The river drains north toward the Chilliwack River at a gradient of 0.005 (Holding and A. 2012). A fish counting fence has existed on Sweltzer River outside the Salmon Research Laboratory with data extending back to the 1920s (Cultus Sockeye Recovery Team 2005). WSC gauge 08MH033 (Sweltzer River at Cultus Lake) was active downstream of the Columbia Valley Highway near the fish counting fence between 1947–1956 and 1960–1964. The drainage area to the gauge location as indicated by WSC is 65 km^2; however, delineation by Shortreed (2007) indicates a drainage area of 75 km^2, which upon further investigation will be taken as correct. The flow is artificially controlled by means of stop logs and a low head weir that maintain a constant water level in Cultus Lake. The two-year flood flow rate is approximately 14.3 $m^3 s^{-1}$ based on a log-Pearson Type III distribution with annual extremes occurring between October and February. The width and maximum depth were 18.3 m and 0.89 m, respectively with a discharge of 2.8 $m^3 s^{-1}$ on 2 November. The bed material consists of coarse sand and gravel.